



**MULTI-STATE HYDRO-PNEUMATIC SUSPENSION SYSTEM THROUGH
THE USE OF MAGNETO-RHEOLOGICAL (MR) VALVES**

by

Jacob Frederick Grobler (10047868)

Submitted in partial fulfilment of the requirements for the degree

Masters (Mechanical Engineering)

in the

Department of Mechanical and Aeronautical Engineering
Faculty of Engineering, Built Environment and Information Technology

UNIVERSITY OF PRETORIA

October 2015

ABSTRACT

MULTI-STATE HYDRO-PNEUMATIC SUSPENSION SYSTEM THROUGH THE USE OF MAGNETO-RHEOLOGICAL (MR) VALVES

by

Jacob Frederick Grobler (10047868)

Supervisor(s): Prof P. S. Els
Department: Mechanical and Aeronautical Engineering
University: University of Pretoria
Degree: Masters (Mechanical Engineering)
Keywords: Vehicle Dynamics, Hydro-Pneumatic Suspension, Magneto-Rheological, Valve

This study is focused on modifying an existing solenoid valve based semi-active hydro-pneumatic spring-damper system using Magneto-Rheological (MR) fluid. The MR fluid's effective viscosity can be altered by application of a magnetic field. Therefore, using a magnetic/MR valve makes it possible to change the state of the system by simply changing the applied magnetic field.

A prototype MR valve was developed to determine whether a unit small enough for installation was possible. This prototype valve was designed from first principles and properties such as pressure drop over the valve (damping) and flow blocking (for switching between spring characteristics) were measured. The measured pressure drop over the valve was higher than what was design for which was due to an incorrect assumption for the viscosity of the thixotropic MR Fluid. The flow blocking ability of the valve was determined by constant force tests. Results showed that the valve could virtually block the flow of fluid for approximately a quarter of the vehicles weight.

With the second prototype, the valve design and magnetic circuit design were improved. Two valves were constructed and implemented on a prototype suspension system. The damping

characteristics of the system were lower than expected, however they can be improved by changing the valve geometry. The base spring characteristics are acceptable, however the higher spring characteristics fail when a high force is exerted on the strut that exceeds the valves flow blocking capability. The response time of the valve is not yet sufficient to make the system viable for real world implementation, especially under extreme conditions that can change more rapidly than the current valves.

ACKNOWLEDGEMENTS

I give thanks to the Lord Jesus Christ for the strength and inspiration He provided during the completion of this study.

Thank you Prof. Els for being an awesome supervisor. Even though we did bump heads sometimes your advice was always considered.

I would also like to thank the Sasol Labs for use of their facilities.

I would like to thank Gerrie Heymans, who is continuing the MR valve research, for his assistance during experimental testing as well as his help during the data analysis.

TABLE OF CONTENTS

Acknowledgements	4
List of Abbreviations	8
List of Symbols	10
List of Figures	10
List of Tables	13
CHAPTER 1 Introduction	1
1.1 Background	2
1.2 Purpose of Research	3
1.3 Problem Statement	3
CHAPTER 2 Literature Review	4
2.1 The Four-State Semi-active Suspension System ($4S_4$)	4
2.1.1 Working Principle of the $4S_4$	4
2.1.2 System Characteristics	6
2.2 Magneto-Rheological (MR) Damper Design for Off-Road Vehicle Suspensions with Flow Blocking Ability	10
2.2.1 Working Principle	13
2.2.2 Valve Characteristics	14
2.3 Overview of Theory and Concepts	15
2.3.1 Magnetic Circuits	21
2.4 Conclusion of Literature Study	25
CHAPTER 3 Magneto-Rheological (MR) Valve Development	26

3.1	Design	26
3.1.1	Properties and Figures used in the Design	27
3.1.2	Design of the annular flow area	30
3.1.3	Design of the magnetic circuit	30
3.1.4	Final Design	32
3.2	Test Setup	32
3.3	Results	34
3.3.1	Flow Blocking	34
3.3.2	Damping	35
3.3.3	Theoretical Model	36
3.3.4	Response Time	38
3.4	Proposed Design Amendments	39
CHAPTER 4 Magneto-Rheological (MR) 4S₄ Development		40
4.1	Magnet Design	40
4.1.1	Magnetic Circuit	40
4.1.2	Magnetic-Electric Circuit Analogy	41
4.1.3	Solution	41
4.2	Experimental Set-up	43
4.2.1	Sensor Descriptions	43
4.2.2	Pressure Measurement based on Thin Pressure Vessel Theory	45
4.3	Conclusion	45
CHAPTER 5 Results		47
5.1	Bulk Modulus	48
5.2	Response Time	49
5.2.1	System Response Time	51
5.3	MR 4S ₄ Spring Characteristics	53
5.3.1	Results for Soft Spring Setting	53
5.3.2	Results for the first Hard Spring Setting	53
5.3.3	Results for the second Hard Spring Setting	54
5.3.4	Observations	56
5.4	MR 4S ₄ Flow Blocking Ability	58
5.5	Damping Tests	59

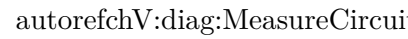
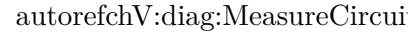
5.5.1	Floating Piston Friction	60
5.5.2	Estimated Spring Characteristic	61
5.5.3	MR $4S_4$ Damping Characteristics	62
5.6	Custom Pressure Sensors	64
5.7	Conclusion of Results	66
CHAPTER 6 Conclusion and Recommendations		68
6.1	Response Time	68
6.2	Magnetic Circuit	69
6.3	Damping	69
6.4	Strain Sensors	71
REFERENCES		73

LIST OF ABBREVIATIONS

MR	Magneto-Rheological
4S ₄	Four State Semi-active Suspension System
MMF	Magneto Motive Force
EMF	Electro-Motive Force

LIST OF SYMBOLS

η	Viscosity	[Pa · s]	Equation 2.1
$\dot{\gamma}$	Shear rate	[1/s]	Equation 2.1
τ_y	Shear yields stress of MR fluid	[Pa]	Equation 2.1
ϕ	Volume fraction of iron particles		Equation 2.2
H	Magnetic field intensity	[A/m]	Equation 2.2
C	Constant $C = [1.0, 1.16, 0.95]$		Equation 2.2
B	Magnetic flux density	[Wb/m ² or T]	Equation 2.3
μ_0	Magnetic permeability of free space ($4\pi \times 10^{-7}$)		Equation 2.4
ΔP_η	Pressure drop due to viscous component	[Pa]	Equation 2.3
ΔP_τ	Pressure drop due to induced yield stress	[Pa]	Equation 2.4
Q	Flow rate through the valve	[m ³ /s]	Equation 2.4
L	Length of the valve	[m]	Equation 2.4
w	Width of the valve	[m]	Equation 2.4
g	Gap of the valve	[m]	Equation 2.4
c	Parameter		Equation 2.4
P	Pressure drop between two plates	[Pa]	Equation 2.5
V	Active fluid volume	[m ³]	Equation 2.6
λ	Control ratio		Equation 2.6
τ	Fluid shear stress	[Pa]	Equation 2.6
k	Factor		Equation 2.6
W_m	Mechanical power dissipation		Equation 2.6
N	Number of windings on a coil		Equation 2.7

I	Current flowing through the coil	[A]	Equation 2.7
l	Length of the solenoid	[m]	Equation 2.7
μ_r	Relative permeability		Equation 2.7
μ	Magnetic permeability		Equation 2.7
L	Coil Inductance	[H]	Equation 2.10
S	Cross sectional area of the loop/coil	[m ²]	Equation 2.8
R	Resistance of the copper coil	[Ω]	Equation 2.9
A_w	Cross sectional area of copper wire	[m ²]	Equation 2.9
ρ	Material resistivity	[Ω · m]	Equation 2.9
T	Inductor time constant	[s]	Equation 2.10
Φ	Magnetic flux	[Wb]	Equation 2.11
\mathcal{F}	Magneto motive force	[A · Turns]	Equation 2.12
\mathcal{R}_m	Reluctance of the magnetic circuit	[A · Turns/Wb]	Equation 2.14
\mathcal{R}	Magnetic element reluctance	[A · Turns/Wb]	Equation 2.15
l	Magnetic element length	[m]	Equation 2.15
A	Magnetic element area	[m ²]	Equation 2.15
L_1	Geometry pressure drop length	[m]	Equation 3.1
L_2	Magnetic field pressure drop length	[m]	Equation 3.1
a	Temperature coefficient		Equation 3.3
p	Scaling factor		Equation 3.3
k	Power law constant		Equation 3.3
q	Scaling factor		Equation 3.4
V_1	Battery voltage measurement	[V]	
			
ΔV_2	Voltage measurement over sense resistor	[V]	
			
V_3	Coil voltage measurement	[V]	Figure 5.3
V_4	Input voltage measurement	[V]	Figure 5.3
R_{in}	Resistor for MOSFET	[Ω]	Figure 5.3
R_T	Total spring resistance		Equation 5.1
R_1	Spring 1 resistance		Equation 5.1
R_2	Spring 2 resistance		Equation 5.1

LIST OF FIGURES

2.1	4S ₄ Circuit Diagram (Els, 2006)	5
2.2	4S ₄ Prototype 2 (Els, 2006)	6
2.3	4S ₄ Soft Spring Characteristics (Els, 2006)	7
2.4	4S ₄ Stiff Spring Characteristics (Els, 2006)	8
2.5	4S ₄ Damping Characteristics (Els, 2006)	9
2.6	MR Microstructure. (Seung-Bok and Young-Min, 2012).	10
2.7	Cutaway of a Delphi MagneRide rear shock absorber with supplementary air spring and a cutaway of a Delphi MagneRide suspension strut. (Delphi, 2005)	11
2.8	Section view of MR Valve Layout (Meeser, 2014)	13
2.9	MR Valve Damping Characteristics (Meeser, 2014)	14
2.10	MR Valve Flow Blocking Ability (Meeser, 2014)	15
2.11	Damping Characteristics of new valve design. (Meeser, 2014)	16
2.12	Shear Yield Stress of MR fluid with 32% volume fraction iron particles	17
2.13	Magnetic Flux Density of MR fluid with 32% volume fraction iron particles	18
2.14	Different modes of operation for controllable fluid devices: (a) Pressure driven flow mode, and (b) direct shear mode. (Carlson and Chrzan, 1994)	19
2.15	B-H Relation for low carbon steel. (MagWeb, 2014)	25
3.1	Optimised High and Low pressure drop <i>vs.</i> characteristics of the 4S ₄ . (Meeser, 2014)	27
3.2	Design point for the magnetic circuit using Equation 2.2	29
3.3	Design point according to fluid saturation.	29
3.4	Geometry determined from the magnetic simulation.	31
3.5	Simulation results for the magnetic field intensity H.	31
3.6	Final Geometry of the prototype MR valve	33
3.7	MR Valve showing MR Fluid Flow and MR Gap	34

3.8	Size comparison between the MR valve by Meeser (Left) and the current prototype (Right)	34
3.9	The test setup showing the red frame and double acting piston.	35
3.10	Experimental results obtained from the Flow Blocking tests.	35
3.11	Combined Damping and Flow Blocking Results with the original theoretical model for the off-state.	37
3.12	Combined Damping and Flow Blocking Results with the adjusted theoretical model for the off-state.	38
3.13	Valve Characteristics due to larger 1.2 mm gap size.	39
4.1	Elements of the magnetic circuit.	41
4.2	Analogous electric circuit for the MR valve.	42
4.3	Numbering and Locations of the sensors used on the suspension during testing.	44
4.4	Cross section of the accumulator sleeve showing the turned down sections where the strain gauges will be placed.	46
4.5	Results of a FEM analysis to determine whether the turned down sections are long enough for uniform stress/strain.	46
5.1	Method used to clean the data.	48
5.2	Pressure-Displacement Data of the Bulk Modulus measurement.	49
5.3	Control Circuit used to measure the magnetic circuit response time.	50
5.4	Typical measure during the time response tests.	50
5.5	System response measurements using the force as measured on the main strut. (Magnets set to 2A each)	52
5.6	MR 4S ₄ Soft spring curve.	53
5.7	MR 4S ₄ first Hard Spring Setting.	54
5.8	Measured pressure values for the second hard spring setting	55
5.9	Measured pressure values for the second hard spring setting	56
5.10	Three different spring settings.	58
5.11	Typical recordings from the flow blocking tests.	59
5.12	Ability of the combined valves to resist the flow of fluid.	60
5.13	Displacement Signal that was used as input to the actuator controller.	60
5.14	Accumulator Floating Piston Friction determined from Off-State damping data.	61

5.15	Force-Displacement data showing it is possible to determine the spring characteristics from damping data.	62
5.16	Force-Velocity Relationship of the MR 4S ₄ Prototype for various current settings.	63
5.17	Force-Displacement Relationship of the MR 4S ₄ Prototype showing how the damping data was extracted.	64
5.18	Force-Velocity Relationship showing a change in damping force mid-stroke.	65
5.19	Small & Large Accumulator MR fluid Pressure showing how fluid flow is temporarily block through the valve of the small accumulator.	65
5.20	Pressure - Strain relation for all strain sensors.	66
6.1	Current Construction of the Magnet.	70
6.2	Proposed new construction of the Magnet.	70
6.3	Design of a possible solution for the high recorded damping forces at low speeds by means of a bypass valve.	71
6.4	Possible implementation of strain gauge sensors to avoid interference.	72

LIST OF TABLES

2.1	Different States of the $4S_4$	5
2.2	Difference between discrete and continues active suspensions (Els, 2006) . . .	12
3.1	Values of the constants used in Equation 3.3, Equation 3.4 and Equation 3.5	38
5.1	Magnet Response Times	51
5.2	System Response Times using the Power Supply	52
5.3	Explanenation of Figure 5.9	57

CHAPTER 1

INTRODUCTION

The research presented in this dissertation aims to overcome the ride comfort *vs.* handling compromise of vehicles. The proposed solution is a semi-active hydro-pneumatic suspension system with continuously variable damping and selectable spring characteristics. The proposed system is based on work done by [Els \(2006\)](#) where he designed and tested a hydro-pneumatic suspension system called the **Four State Semi-Active Suspension System**, or **4S₄**. With this system he achieved different damping characteristics as well as spring characteristics by making use of solenoid valves. The proposed solution will attempt to achieve this by making use of Magneto-Rheological (**MR**) fluid.

The first milestone of the research was to determine whether it is possible to build an MR valve which can provide continuously variable damping as well as block the flow of fluid through the valve (or at least a very low flow rate) and be small enough to implement practically. Therefore, a prototype valve was designed, of which the size envelope was acceptable, and tested. Results showed that the damping range of valve was slightly higher than the desired, however this could easily be rectified with a second prototype. The valve also exhibited the ability to virtually block the flow of fluid up and to a certain pressure drop over the valve where after the valve began to “leak” excessively.

These results proved favourable enough to continue with a second prototype valve as well as a full suspension prototype. Salvaging parts from a previous suspension and designing a new valve block which included the MR valves the new system was tested and analysed. Results showed that the damping range was this time below the desired range due to the fluid flow being split between the two valves. The ability of the valves to block the flow fluid

was comparable to that of the first valve prototype even though the annular area was slightly larger.

The concept as a whole holds much promise even at these early stages in development, however at the conclusion of this research only a few questions were answered and many more new questions arose which still needs to be answered. In effect it is still too early in the development phase to either dismiss the concept or give it a stamp of approval.

1.1 BACKGROUND

Suspensions have come a long way since the earliest introduction of simple leaf springs. Later on the adoption of dampers and coil springs gave rise to smaller suspensions which provided a much more comfortable driving experience. Later on air/pneumatic springs were introduced into vehicles, trucks, cabin suspensions and military vehicles of which the spring characteristics could be changed.

The first dampers were known as passive dampers, later on terms such as semi-active suspension as well as active suspensions were also used to classify the different suspensions in industry. The bulk of the vehicle market uses passive dampers, that is why they suffer from the ride comfort vs. handling compromise whereas the select few makes use of semi-active dampers and even less makes use of active dampers. Dampers that makes use of bypass valves or more recently magneto-rheological (MR) fluid are examples of semi-active dampers. Active suspension makes use of actuators that can continuously control the forces acting on the vehicle.

The **Four State Semi-Active Suspension System**, or $4S_4$, on which the current research is based is a semi-active system that switches between four different states of which there are two damping and two spring characteristics. The purpose of the $4S_4$ originally was to improve the ride comfort and handling capabilities of a Land Rover Defender 110. However the Defender 110 only served as the test platform and the intended use is on larger off-road vehicles that has a large mass difference between fully laden and empty.

1.2 PURPOSE OF RESEARCH

As mentioned already, Els (2006) developed a system called the Four State Semi-Active Suspension Systems, or $4S_4$. This system however suffers from some limitations.

The first is that the solenoid valves used become impractical when large flow rates are required. The second is that the response times of affordable valves are not yet good enough.

The purpose of this research is to investigate the feasibility of replacing the solenoid valves with MR valves that can also block the flow of fluid. MR fluid blocking capability was shown by Meeser (2014) to be feasible, but the valve was bulky and had slow response times. This research aims to determine whether it is possible to develop a MR valve with the ability to virtually block the flow of fluid to ultimately replace the solenoid valves currently in the $4S_4$.

1.3 PROBLEM STATEMENT

The problem statement is therefor to design, develop, test and model a $4S_4$ suspension system using Magneto-Rheological fluid that can:

1. Provide continuously variable semi-active damping
2. Block flow so that spring characteristics can be changed by blocking out accumulators
3. Switch fast enough for effective semi-active suspension control.

CHAPTER 2

LITERATURE REVIEW

Section 2.1 gives a detailed description of the working principles and characteristics of the 4 State Semi-Active Suspension System (or $4S_4$). Section 2.2 discusses the flow blocking capabilities of Magneto-Rheological (MR) valves. Section 2.3 covers the necessary theory, concepts and fluid properties relevant to the development of MR valves.

2.1 THE FOUR-STATE SEMI-ACTIVE SUSPENSION SYSTEM ($4S_4$)

The **Four State Semi-active Suspension System** ($4S_4$) was developed as a possible solution to the ride comfort vs. handling compromise. The $4S_4$ switches between two discrete spring characteristics and between two discrete damping characteristics. These discrete states can achieve either a very soft suspension which is commonly associated with very good ride comfort or a firm suspension commonly used in sports cars for better handling performance (Els, 2006).

2.1.1 Working Principle of the $4S_4$

Figure 2.1 shows a basic schematic diagram of the $4S_4$ prototype. The figure depicts the gas accumulators, damper packs as well as the different locations of the solenoid valves (ON-OFF Valves). The two gas accumulators provide the two different spring characteristics and can be finely tuned by changing the mass of gas loaded into each accumulator. The two damper packs are standard orifice and shim based valves salvaged from old dampers that gave the required characteristics.

Table 2.1 depicts the four states of the $4S_4$ together with the different valve positions. Els

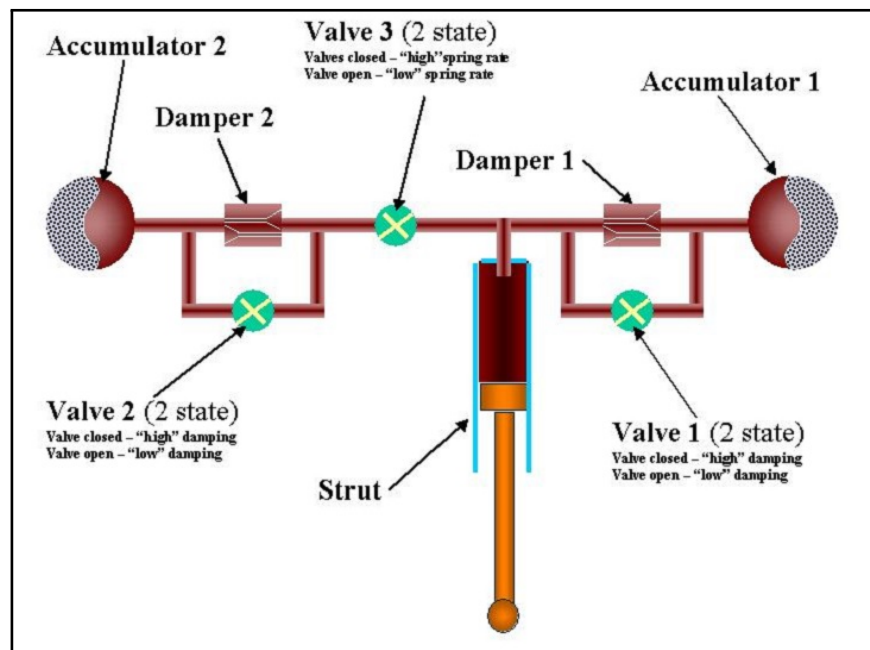


Figure 2.1: $4S_4$ Circuit Diagram (Els, 2006)

used only two of the four states namely low spring, low damping for good ride comfort and high spring, high damping for good handling.

Table 2.1: Different States of the $4S_4$

	Valve 1	Valve 2	Valve 3
Low Spring, Low Damping	Open	Open	Open
Low Spring, High Damping	Closed	Closed	Open
High Spring, Low Damping	Open	Open	Closed
High Spring, High Damping	Closed	Closed	Closed

The low spring characteristic is achieved by compressing the combined volume of the two gas accumulators. The higher spring characteristic is achieved by sealing off accumulator 2 (closing valve 3). The high and low spring characteristics can be independently adjusted over a wide range by controlling the mass of gas in each accumulator during the gas charging process. Each damper pack has a bypass valve. For low damping both bypass valves (valves 1 and 2) are set to the open position. In this case the damping characteristic is largely determined by the pressure drop over the bypass valves. For high damping both valves are

set to the closed position forcing the fluid through the damper packs. This high damping characteristic is determined by the characteristic of the damper packs. (Els, 2006)

2.1.2 System Characteristics

Figure 2.2 shows the prototype of the $4S_4$ developed by Els (2006). The figure indicates the locations of the accumulators, solenoid valves, valve block and all the other components.

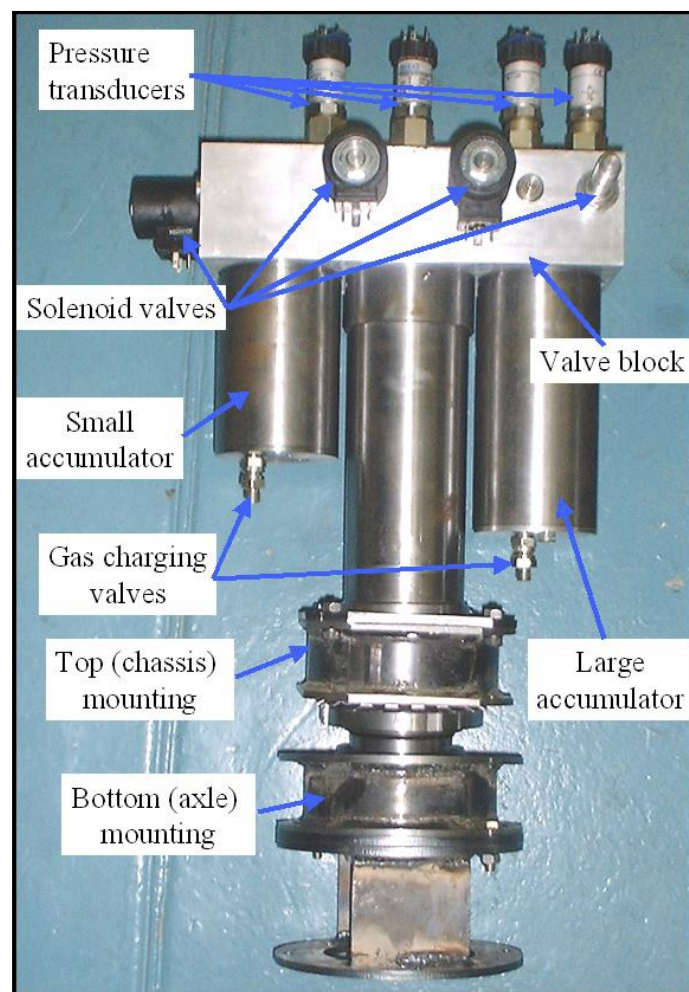


Figure 2.2: $4S_4$ Prototype 2 (Els, 2006)

The $4S_4$ prototype was characterised using a Shenck Hydrapulse actuator and was mounted on a special test rig. Various characteristics of the $4S_4$ were determined by Els (2006) and used as input to develop a mathematical model of the system.

Spring Characteristics

The spring characteristics were determined by displacing the strut very slowly to eliminate damping.

Figure 2.3 shows the soft spring characteristics measured for one complete compression and rebound cycle. Els (2006) also compared the spring characteristic to the predicted isothermal spring characteristics calculated for a static gas volume of 0.5 litres and shows that excellent correlation is achieved.

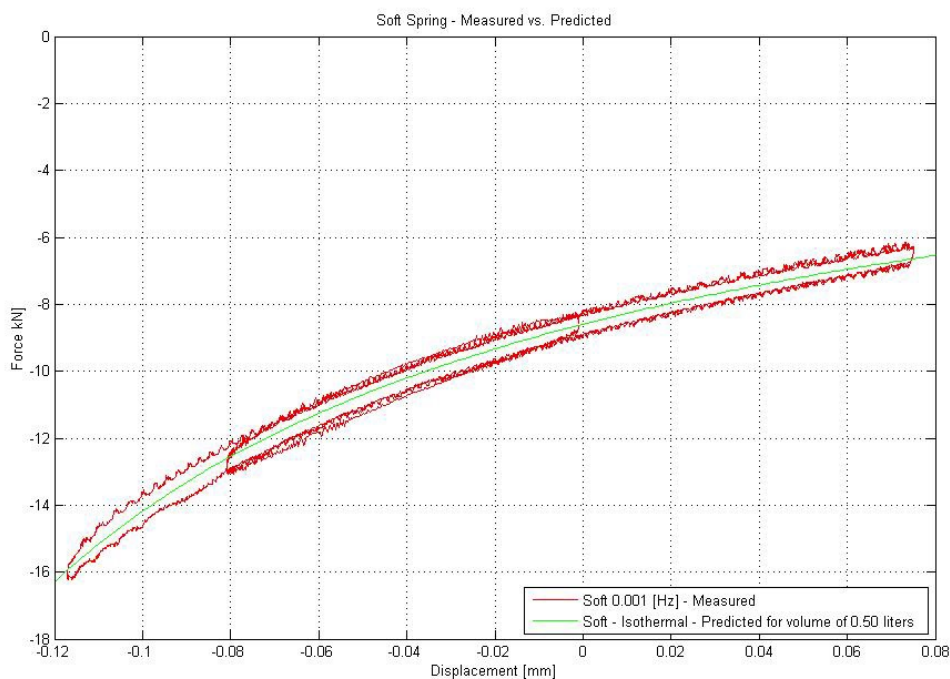


Figure 2.3: 4S₄ Soft Spring Characteristics (Els, 2006)

Figure 2.4 shows the stiff spring characteristic measured for a complete compression and rebound cycle. When a comparison was done between the measured values and the isothermal spring characteristics Els (2006) noticed a discrepancy between the two data sets. On further investigation it was discovered that for the stiff spring the compressibility of the fluid is not negligible. Adding the effect of the experimentally determined bulk modulus in the calculations, as indicated in Figure 2.4, resulted in very good correlation.

Both soft and stiff spring characteristics (Figure 2.3 and Figure 2.4) indicated a hysteresis

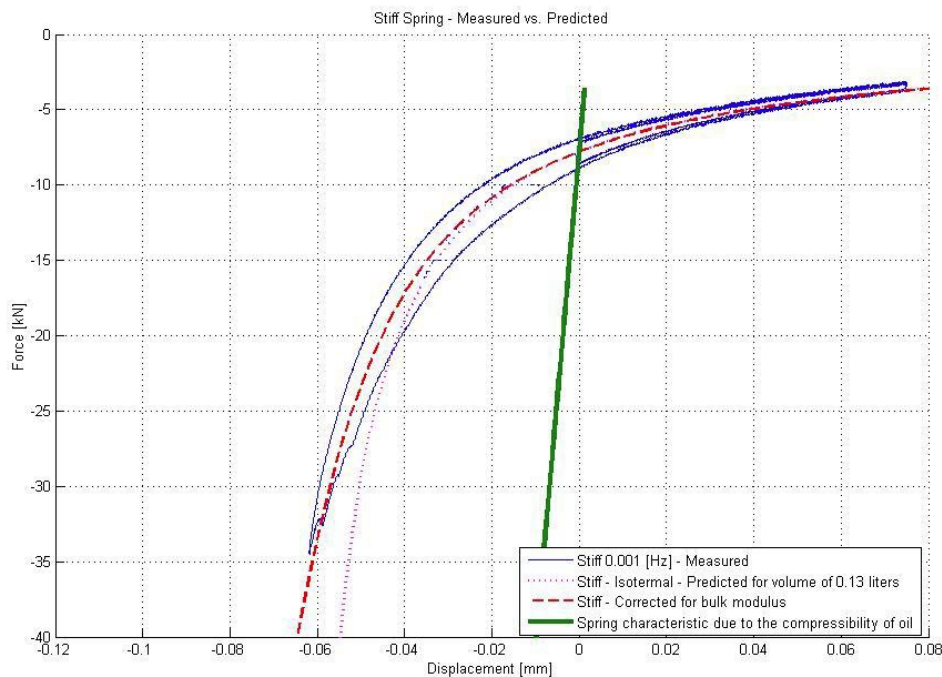


Figure 2.4: $4S_4$ Stiff Spring Characteristics (Els, 2006)

loop. The biggest contribution to hysteresis in the soft spring characteristic is friction between the cylinder and seals. A second, very important effect, namely heat transfer between the gas and surroundings, as well as the fact the the ideal gas approach is not valid for the high pressures encountered, was taken into account by Els (2006) using a real gas equation of state as well as a thermal time constant heat transfer model.

Damping Characteristics

Els (2006) states that the most important damper characteristic, as far as vehicle dynamics is concerned, is the force velocity relationship of the high damping and low damping characteristics respectively as measured using a triangular wave displacement input at various frequencies.

Figure 2.5 shows the force-velocity relationships for the stiff spring with low damping, stiff spring with high damping as well as the soft spring with low damping as measure by Els.

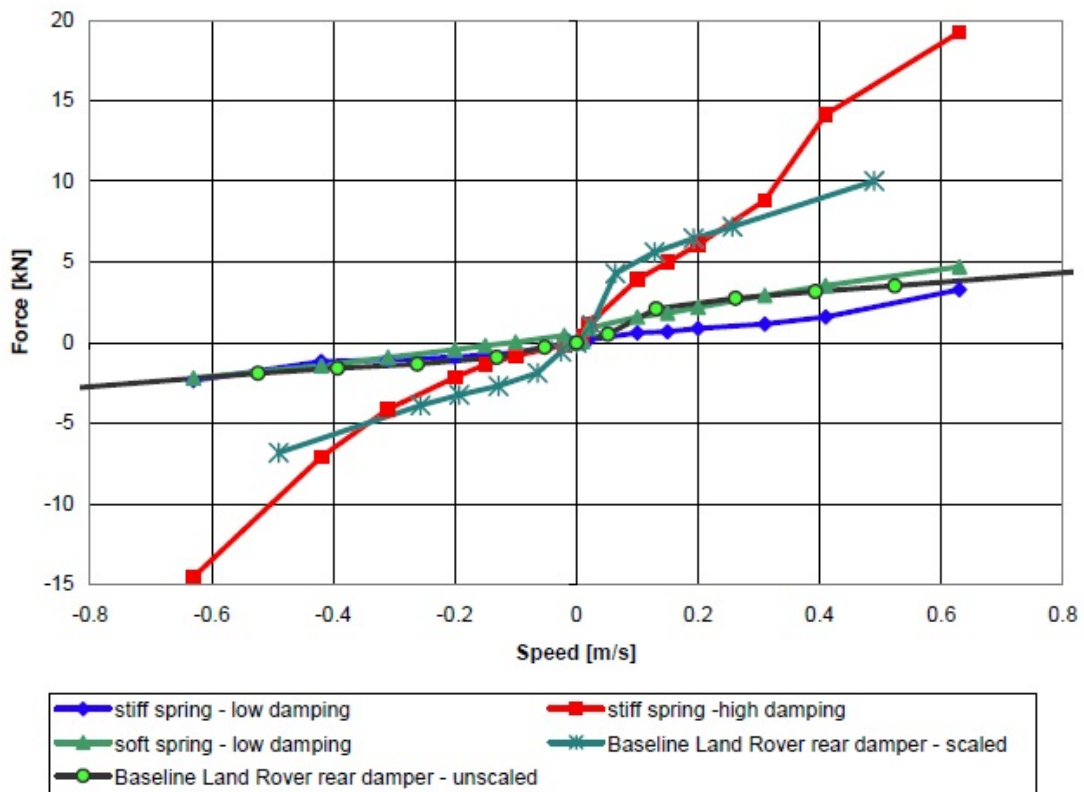


Figure 2.5: $4S_4$ Damping Characteristics (Els, 2006)

Valve Response Time

The final property of note is the response time of the valves. Els (2006) states that valve response times are very important for predicting the transient response of the system to valve switching. For enough severe manoeuvres in the real world it is required that the response of the valves be quick for the control system to be effective.

The response time used was the 5 - 95% value to ensure that the full damping effect is captured. The switching time of the system ranged from 40 - 90 milliseconds and is largely due to the transient characteristics of the on-off solenoid valves used in the prototype.

2.2 MAGNETO-RHEOLOGICAL (MR) DAMPER DESIGN FOR OFF-ROAD VEHICLE SUSPENSIONS WITH FLOW BLOCKING ABILITY

Magneto-Rheological (MR) Fluids

Magneto-Rheological (MR) fluids are suspensions of magnetized micron-sized iron particles in a dispersing liquid. When an external magnetic field is applied, the particles acquire magnetic moments and attract to each other due to dipolar forces and form anisotropic aggregates aligned with the magnetic field direction. Thus, upon an application of a magnetic field, MR fluids undergo a reversible jamming responsible for several orders of magnitude increase in effective viscosity and the appearance of a yield stress. This phenomenon is also referred to as the magneto-rheological (MR) effect. (Wereley, 2014)

When the magnetic field is applied, the interaction between the resulting induced dipoles causes the particles to form columnar structures, parallel to the applied field (See Figure 2.6). These chain-like structures restrict the motion of the fluid, thereby increasing the viscous characteristics of the suspension. The mechanical energy needed to break these chain-line structures increases as the applied field increases resulting in a field dependent yield stress. Magneto-Rheological fluids has the ability to provide simple, quiet, and rapid-response interfaces between electronic controls and mechanical systems. (Jolly et al., 1999)

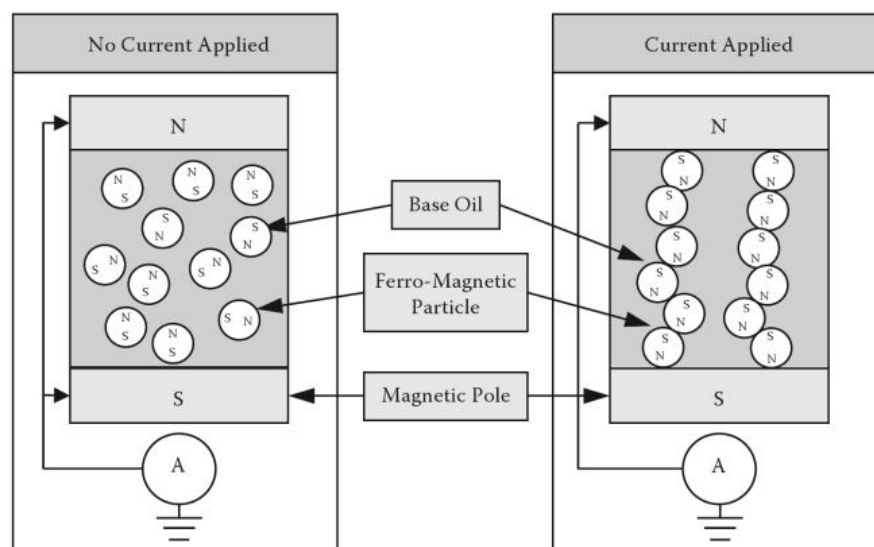


Figure 2.6: MR Microstructure. (Seung-Bok and Young-Min, 2012).

Magneto-Rheological (MR) Dampers

Magneto-Rheological or Magneto-Resistive Dampers are semi-active dampers that can change the amount of resistive damping force upon the application of a magnetic field. This phenomenon is possible due to the MR fluid present in the damper. The application of the magnetic field increases the apparent viscosity, or shear stress of the MR fluid which in turn increases the resistance of the fluid to deformation, this is known as the MR effect. A detailed discussion of the properties of MR fluid is presented in the next chapter.

MR dampers are used in seat suspensions, vehicle cabin suspensions, anti-seismic applications, weapons recoil dampening, vehicle suspensions, landing gear and probably many more applications. In this study however we will mainly focus on the properties and applications of MR dampers in vehicle suspensions.

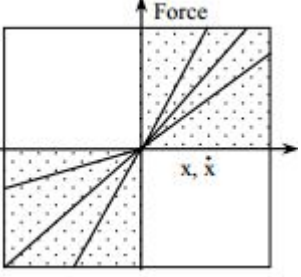
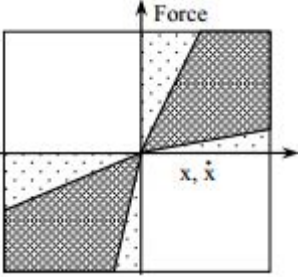
Figure 2.7 shows an example of an MR damper developed by Delphi for application in vehicle suspensions. MR dampers belongs to the semi-active continuous suspension system category whereas the $4S_4$ belongs to the semi-active discrete category. The difference between the two is that the one can quickly and continuously vary between certain limits while the latter can only change between discrete values very quickly.



Figure 2.7: Cutaway of a Delphi MagneRide rear shock absorber with supplementary air spring and a cutaway of a Delphi MagneRide suspension strut. (Delphi, 2005)

Table 2.2 shows the difference between the discrete and continuous semi-active classes.

Table 2.2: Difference between discrete and continuous active suspensions (Els, 2006)

Class	Forces
Semi-active: Discreet	
Semi-active: Continuous	

These systems provide superior control yet they are still mostly used on high end vehicles. This is because the relative cost of the system compared to the vehicle is quite high. However, it can be argued that with an increase in the size of the vehicle, ex. mining equipment, the relative cost of the MR system would become much more attractive and the added benefits could out way the added extra cost. Therefore the decision was made to conduct research into the possibility of using MR technology as a replacement for the solenoid valves in the $4S_4$.

Meeser (2014) made the first attempt at replacing the solenoid valves in the $4S_4$ prototype with a Magneto-Rheological (MR) valves. Part of the requirements for the MR valve to replace the solenoid valve is the ability to block the flow of fluid. This ability is needed to change the spring rates as well as lock the suspension during severe handling manoeuvres.

Meeser showed that it was indeed possible to virtually block the flow of fluid. The flow of fluid however cannot be completely blocked in the valve since there is no physical block and an effective increase in viscosity cannot be that large. What does happen is that the flow of fluid becomes so slow that the suspension travel is negligible during a severe handling manoeuvre. However, for the change in spring characteristics the low flow is still too large

over a long period especially when a change in spring characteristics is desired.

2.2.1 Working Principle

The Magneto-Rheological (MR) valve designed by Meeser uses the the valve mode of operation also known as the pressure driven flow mode. [Figure 2.8](#) shows a cross-sectional view of the MR valve developed and tested by Meeser.

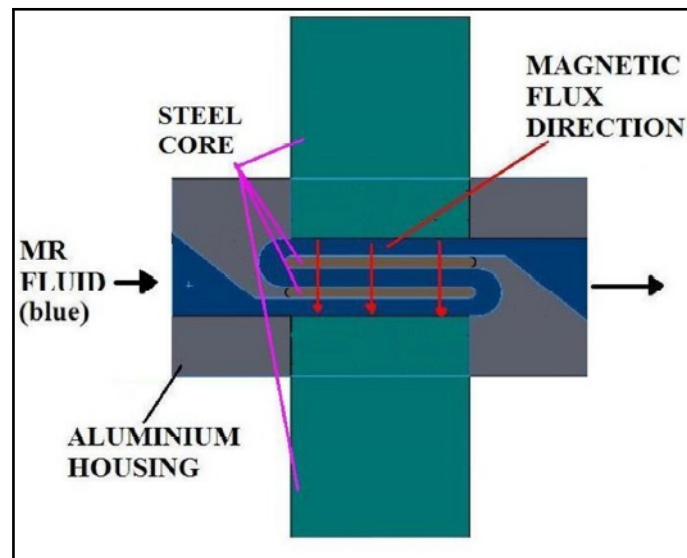


Figure 2.8: Section view of MR Valve Layout ([Meeser, 2014](#))

Meeser's design is a classical valve mode, meaning that the cross-sectional area is rectangular with width, length and thickness such as in the definition. Using the basic formula for pressure drop over a valve [Meeser](#) determined that a valve with a length of 120 mm, a width of 40 mm and a gap thickness of 2.5 mm would meet the requirement for both the on- and off-state damping.

In order to make the valve more compact [Meeser](#) split the valve into three regions and stacked them on top of each other. This also makes the area where the magnetic field is applied smaller and allows for theory that considers magnetic field lines perpendicular to the flow of fluid.

2.2.2 Valve Characteristics

Damping

Figure 2.9 shows a direct comparison of the MR valve simulated by Meeser and the optimised $4S_4$ characteristics. From the figure it is clear that for low flow rates the MR valve exceeds the upper limit of the $4S_4$, however with an increase in flow rate the upper limit of the $4S_4$ cannot be reached by the MR valve. The only way to correct this is to increase the slope of the curve in the off-state of the MR valve where off-state refers to an fully de-energized magnet and on-state refers to an energized magnet. However increasing the slope too much adds the risk to exceed the lower limit of the $4S_4$ at high flow rates. It is a trade-off that has to be carefully considered. Note, the area in the figure representing the MR Valve is that of the valve model determined by Meeser.

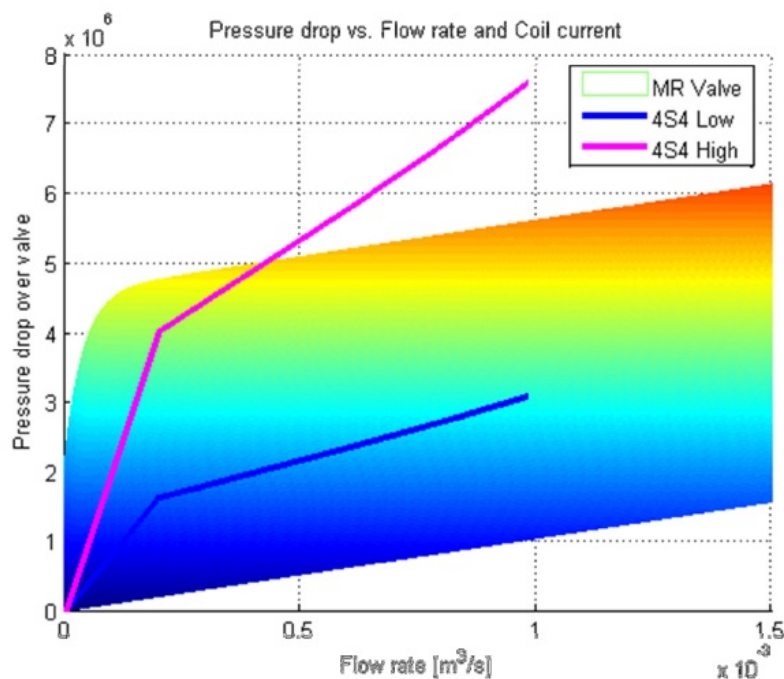


Figure 2.9: MR Valve Damping Characteristics (Meeser, 2014)

Flow Blocking

Figure 2.10 shows the results of the flow blocking or low flow rate test that Meeser performed. The figure shows that the MR valve can withstand a suspension force of just under 4 kN

without a significant flow rate.

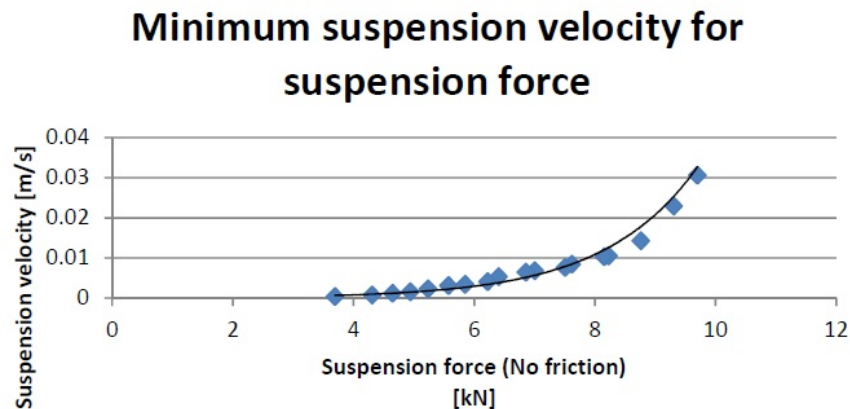


Figure 2.10: MR Valve Flow Blocking Ability (Meeser, 2014)

Remarks

As was seen in Figure 2.9 the MR valve could not reach the upper limit of the optimised $4S_4$ at high flow rates. Meeser therefore recommended a new design with a smaller fluid gap of 2 mm to reach the upper limit as shown in Figure 2.11. In the off-state there was only an increase in the slope due to the smaller fluid gap. However, the smaller fluid gap provides much less magnetic resistance in the on-state and results in a stronger magnetic field across the gap. With the stronger magnetic field the MR effect is much greater as well as the resulting pressure drop across the valve.

The one major drawback with the valve that was design by Meeser was the size. Even though the valve did perform quite well the size of the device made it impractical for a full implementation on the $4S_4$. The response time of the valve is also unknown.

2.3 OVERVIEW OF THEORY AND CONCEPTS

This section provides a quick reference describing the terminology and functioning of MR fluids and devices as well as the magnetic circuits.

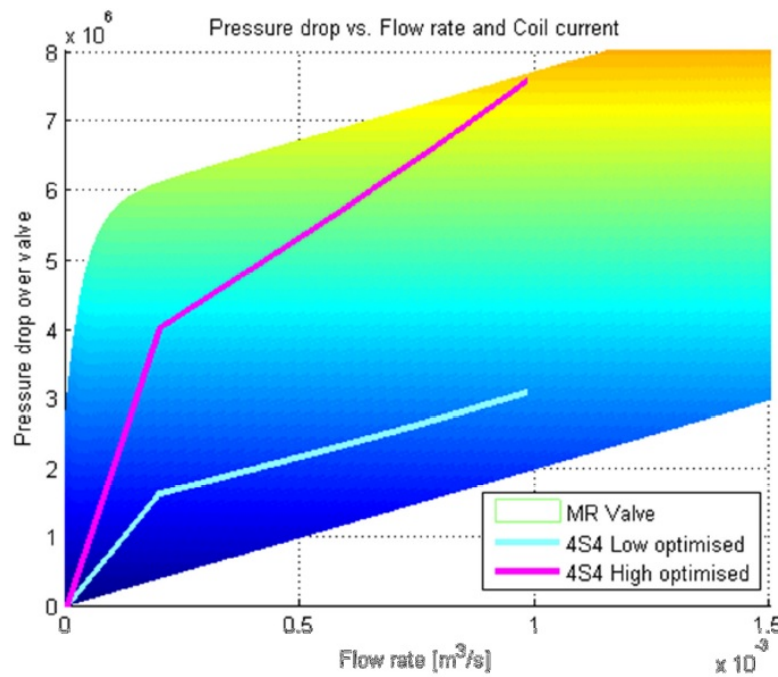


Figure 2.11: Damping Characteristics of new valve design. (Meeser, 2014)

Magneto-Rheological (MR) Fluid Models and Properties

From a fluid mechanics point of view, the behaviour of MR fluids in the absence of a magnetic field can be described as Newtonian, while it exhibits distinct Bingham behaviour in the presence of a magnetic field. (Carlson et al., 1996)

Therefore MR fluids have been modelled in general as a Bingham fluid whose constitutive equation is given by the following:

$$\tau = \tau_y + \eta \dot{\gamma} \quad (2.1)$$

where η is the dynamic viscosity, $\dot{\gamma}$ is the shear rate, and $\tau_y(\cdot)$ is the dynamic yield stress of the MR fluid.

Under a magnetic potential, the total shear stress consists of two components - viscous-induced stress and field-dependent yield shear stress. *Note that the magnetic field could be expressed by either magnetic flux density (B) or magnetic field intensity (H). This will be discussed later.* (Seung-Bok and Young-Min, 2012)

MR Fluid Shear Yield Stress

MR fluids has an achievable shear yield stress of $50 - 100\text{kPa}$. They are also not sensitive to impurities or contaminants that may be encountered during their manufacture and operation.

The field dependent yield shear stress can be determined using "Dr. Dave's" empirical equation for MR fluid shear yield stress,

$$\tau_{MR} = C \cdot 27170\phi^{1.5239} \cdot \tanh(6.33 \times 10^{-6} \cdot H) \quad (2.2)$$

where ϕ is the volume fraction of iron particles, τ_{MR} is in Pa, H is in A/m and the constant C equals 1.0, 1.16 or 0.95 depending on whether the carrier fluid is hydrocarbon oil, water or silicon oil. (Carlson, 2005)

Figure 2.12 shows the shear yield stress curve for a MR fluid with 32% volume fraction iron particles.

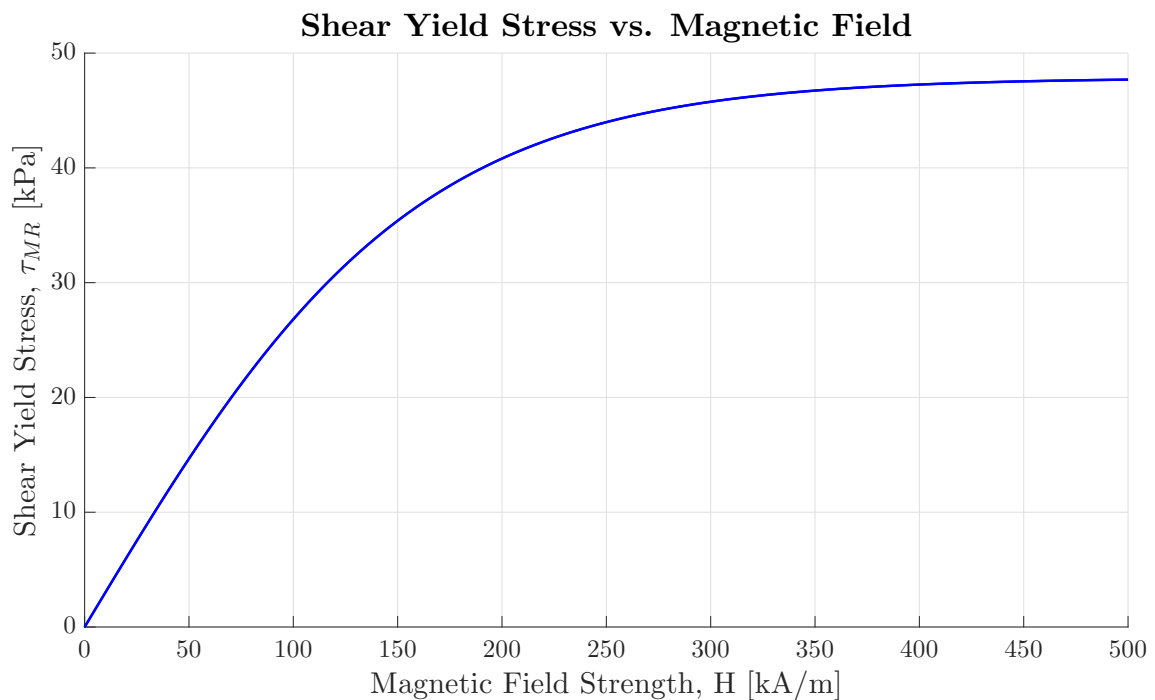


Figure 2.12: Shear Yield Stress of MR fluid with 32% volume fraction iron particles

MR Fluid Magnetic Properties

In order to accurately predict the MR fluid behaviour under the application of a magnetic field, the magnetic properties - such as the magnetic flux density (B) *vs.* magnetic field intensity (H) - of the fluid also needs to be known. This is however difficult, because even though we might know the properties of the suspended iron particles, the fluid magnetic properties are not the same.

These properties however can be modelled using Dr. Dave's empirical equation for the magnetic flux density (B),

$$B = 1.91 \cdot \phi^{1.133} \cdot [1 - \exp(-10.97 \cdot \mu_0 \cdot H)] + \mu_0 \cdot H \quad (2.3)$$

where μ_0 is the magnetic constant equal to $4\pi \times 10^{-7}$ and B is in T (Tesla). (Carlson, 2005)

Figure 2.13 shows the B-H curve for the same 32% volume fraction fluid.

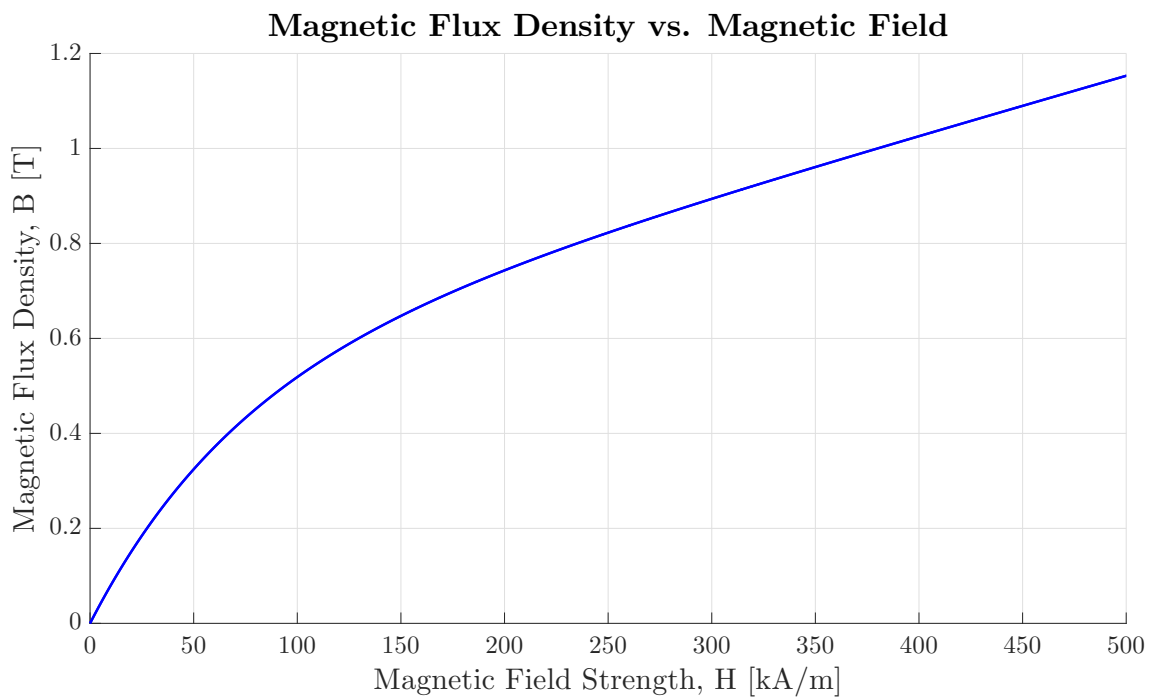


Figure 2.13: Magnetic Flux Density of MR fluid with 32% volume fraction iron particles

Dr. Dave's equations have been developed to provide a practical and convenient description of virtually any MR fluid.

Modes of Operation

There are three modes of operation for MR fluids. The most popular the pressure driven flow mode which has fixed poles. The second the direct shear mode where the poles can move relative to each other. The third the squeeze-film mode where the poles are forced closer to each other.

Figure 2.14 gives a graphical representation of the first two flow modes.

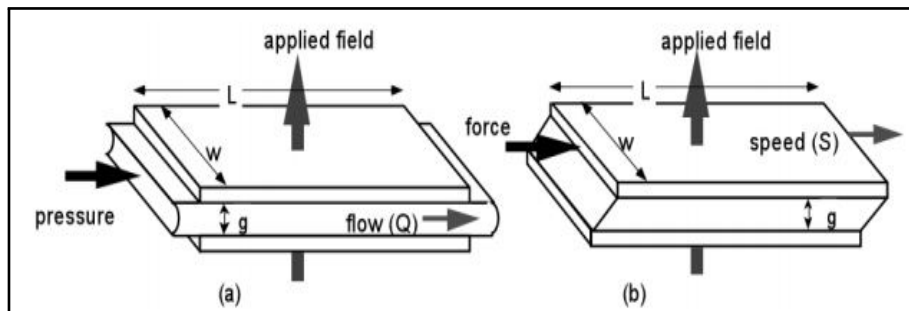


Figure 2.14: Different modes of operation for controllable fluid devices: (a) Pressure driven flow mode, and (b) direct shear mode. (Carlson and Chrzan, 1994)

Pressure Drop Over the valve

As mentioned earlier, it is convenient to have the pressure drop *vs.* flow rate properties of a valve as it does not limit the design to one specific application. As it turns out, devices that uses fluids with a variable yield stress is also designed for pressure drop where the pressure drop is a function of the geometry, fluid properties and the flow rate.

Phillips (1969) provides an equation that can approximate the pressure drop developed in a device based on pressure driven flow mode. This pressure drop is commonly assumed to result from the sum of a viscous component ΔP_η and a field dependent induced yield stress component ΔP_τ . The relation is as follows,

$$\Delta P = \Delta P_\eta + \Delta P_\tau = \frac{12\eta QL}{g^3 w} + \frac{c\tau_y(H)L}{g} \quad (2.4)$$

where L, g and w are the length, gap and width of the flow channel between the fixed poles, Q is the volumetric flow rate, η is the viscosity with no applied magnetic field and τ_y the yield stress developed in response to an applied field H. The parameter c is a function of the

flow velocity profile and has a value ranging from a minimum of 2 (for $\Delta P_\tau/\Delta P_\eta$ less than ~ 1) to a maximum of 3 (for $\Delta P_\tau/\Delta P_\eta$ greater than ~ 100). (Jolly et al., 1999)

Dixon (2007) also presents a model for Bingham flow between two plates in the form of a cubic equation for the pressure drop,

$$P^3(g^3) + P^2 \left(-3L\tau_y g^2 - 12 \frac{\eta L Q}{w} \right) + P^1(0) + P^0(4L^3\tau_y^3) = 0 \quad (2.5)$$

Where the maximum of the several real solutions is the correct one.

Minimum Active Fluid Volume

The minimum active fluid volume of a MR device can be used during the initial stages of the design. It gives the necessary active fluid volume in order to achieve the desired control ratio at a required controllable mechanical power level.

The minimum active fluid volume is obtained by algebraically manipulating Equation 2.4 (Duclos, 1988; Carlson and Chrzan, 1994)

$$V = k \left(\frac{\eta}{\tau_y^2} \right) \lambda W_m \quad (2.6)$$

where k is a constant and $V = Lwg$ can be regarded as the necessary active fluid volume in order to achieve the desired control ratio λ at a required controllable mechanical power level W_m . For pressure driven flow: $k = 12/c^2$, $\lambda = \Delta P_\tau/\Delta P_\eta$ and $W_m = Q\Delta P_\tau$. It is important to note that the minimum active fluid volume is proportional to the product of three terms: a term that is a function of fluid material properties (η/τ_y^2); the desired control ratio or dynamic range; and the controlled mechanical power dissipation sought.

Response Time

The response time of a MR fluid is typically a few milliseconds and the impact is small compared to MR device/damper. (LORD, 2014)

The response time of an MR device is a function of the magnetic circuit, the current controller to energize the magnet and the valve design. The response time is also characterized in a few ways: 1) the time required to build the shear strength in the fluid; 2) the required for the magnetic circuit to energized. There are also two value that can be obtained from a single

measurement: 1) 63.2% response time which is commonly used to measure the time constant of electronic circuits and 2) the 5 - 95 % response time. A MR device's response time can therefore be characterized in 4 different ways.

2.3.1 Magnetic Circuits

The magnetic circuit for the MR device has two major functions. Its first function is to generate the magnetic field in the MR fluid to achieve the desired MR effect. The second is that the magnetic circuit is responsible for the response time of the MR device. The magnetic circuit is much slower in response compared to the MR fluid. There is a trade-off however, the larger the required magnetic field, the slower the response time, then there is also the current supply limitation. It is possible to generate a large enough field in a very short amount of time given a coil with thick enough wire and an ample current supply. The necessary theory and principles pertaining to coil and magnetic circuit design will be discussed in this section.

The Solenoid

The magnetic solenoid or coil can be described as a single length of copper wire that is tightly wound onto a bobbin. When a current passes through the copper wire a magnetic field is generated with the magnetic field line directions determined by the right hand rule. The coil also makes a significant contribution to the response time of the MR device. Only a few parameters are needed to design a coil, like number of turns N , coil length l , the current flowing through the coil I and the thickness of the wire.

Coil Current Density

The current that can flow through a copper wire is limited by the cross sectional area of the wire. Copper wires - as do most conductors - has a certain current density limit. Another limiting factor is the amount of power dissipated by the copper wire, for example a wire insulated with silicon can dissipate much more energy than a wire that is insulated with a thin varnish layer and tightly wound around a bobbin.

In practice the maximum current density can vary from 2.5 A/mm^2 for a wire isolated from

free air to 6 A/mm^2 for a wire in free air. As a general guideline in transformer design, 4 A/mm^2 is regarded as a good current density. It is also recommended to never go above 6.7 A/mm^2 .

Magnetic Field in a Solenoid

The magnetic flux density \mathbf{B} in the interior region of a tightly wound solenoid with N turns, carrying a current I and length l is calculated as follows (Ulaby et al., 2010),

$$B = \frac{\mu NI}{l} \quad (2.7)$$

where $\mu = \mu_r \mu_0$, with μ_r the relative permeability of the solenoid core and $\mu_0 = 4\pi \times 10^{-7}$ the permeability of free space.

Inductance of a Solenoid

The response time of a solenoid is governed in part by the inductance of the solenoid. For a solenoid the inductance L is given as (Ulaby et al., 2010),

$$L = \mu \frac{N^2}{l} S \quad (2.8)$$

where L is in Henry's (H) and S is cross sectional area of the loop/coil.

When the inductance of a solenoid is calculated the core material is also taken into account.

Resistivity of Copper

Electrical resistivity ρ is an intrinsic property that quantifies how strongly a given material opposes the flow of electric current. Using the resistivity of copper we can calculate the resistance of the copper wire/ or coil using Pouillet's law,

$$R = \rho \frac{l}{A_w} \quad (2.9)$$

where ρ is in $\Omega \cdot m$, l is the length of the wire and A_w is the cross sectional area of the wire.

The resistivity of copper at $20^\circ C$ is given as $\rho = 1.68 \times 10^{-8}$.

Time Constant of an Inductor

In the present case an inductor can be regarded the same as a coil/solenoid. Difference being that the solenoid has a core.

The time constant of an inductor or electric circuit is defined as the time it takes to reach the 63.2% level of the steady state current and is calculated as follows,

$$T = \frac{L}{R} \quad (2.10)$$

where T is in seconds, L is in Henry and R is the total circuit resistance in Ohms.

Magnetic Circuit

The magnetic circuit is analogous to an electric circuit with resistors, a power source and the current through the circuit. In a magnetic circuit the resistors are the materials through which the magnetic field is conducted, the power source is the coil or solenoid and the current through the circuit is the magnetic flux. An important concept to grasp is that in a magnetic circuit, the magnetic flux Φ stays constant throughout the circuit whereas the magnetic flux density B can vary as it is dependent on the cross sectional area of the conductor. The relation between the magnetic flux and magnetic flux density is as follows

$$\Phi = B \cdot S \quad (2.11)$$

In an electric circuit, for current to flow there needs to be a closed loop or path for the current to follow. The same reasoning governs the flow of magnetic flux in a magnetic circuit, and as with an electric current the flux will choose the path of least resistance (or reluctance).

Magneto Motive Force (MMF)

Similar to the way that electromotive force (EMF) drives a current of electrical charge in an electrical circuit, MMF 'drives' magnetic flux through magnetic circuits. The MMF around a closed loop is defined as

$$MMF = \mathcal{F} = \oint H \cdot dl \quad (2.12)$$

The term MMF is only an analogy to EMF, because it is not a force nor is anything moving.

The MMF can also be calculated using Ampère's law,

$$\mathcal{F} = NI \quad (2.13)$$

where N is the number of turns and I is the current in the coil.

Another way to calculate the MMF is by means of the Hopkinson's law,

$$\mathcal{F} = \Phi \mathcal{R}_m \quad (2.14)$$

where \mathcal{F} is the magneto motive force across a magnetic element, Φ is the magnetic flux, in Weber (Wb), through the magnetic element and \mathcal{R}_m is the magnetic reluctance, with units [1/Henry], of that element or circuit.

Reluctance

Magnetic reluctance is analogous to resistance in an electrical circuit. The reluctance of a magnetically uniform magnetic circuit element can be calculated as,

$$\mathcal{R} = \frac{l}{\mu A} \quad (2.15)$$

where l is the length of the element in meters (m) and A is the cross sectional area of the circuit element in m^2 .

An important concept to remember is that the reluctance in a magnetic circuit is not constant and that at high magnetic fluxes the magnetic element can begin to saturate. This arises from the fact that the permeability of a magnetic element is also not constant (See [Figure 2.13](#)).

Magnetic Permeability

Permeability is the measure of the ability of a material to support the formations of a magnetic field within itself.

Permeability relates the magnetic flux density B and the magnetic field H with the following expression

$$B = \mu H \quad (2.16)$$

The relative permeability μ_r of a magnetic element is the ration of the permeability of a specific medium to the permeability of free space,

$$\mu_r = \frac{\mu}{\mu_0} \quad (2.17)$$

where $\mu_0 = 4\pi \times 10^{-7}$ is the permeability of free space.

However the relationship between the flux density and magnetic field is not a linear one as [Equation 2.16](#) suggests. Instead it is a nonlinear relation unique for every magnetic material. This can be seen in [Figure 2.15](#) which shows the BH relation for a low carbon steel.

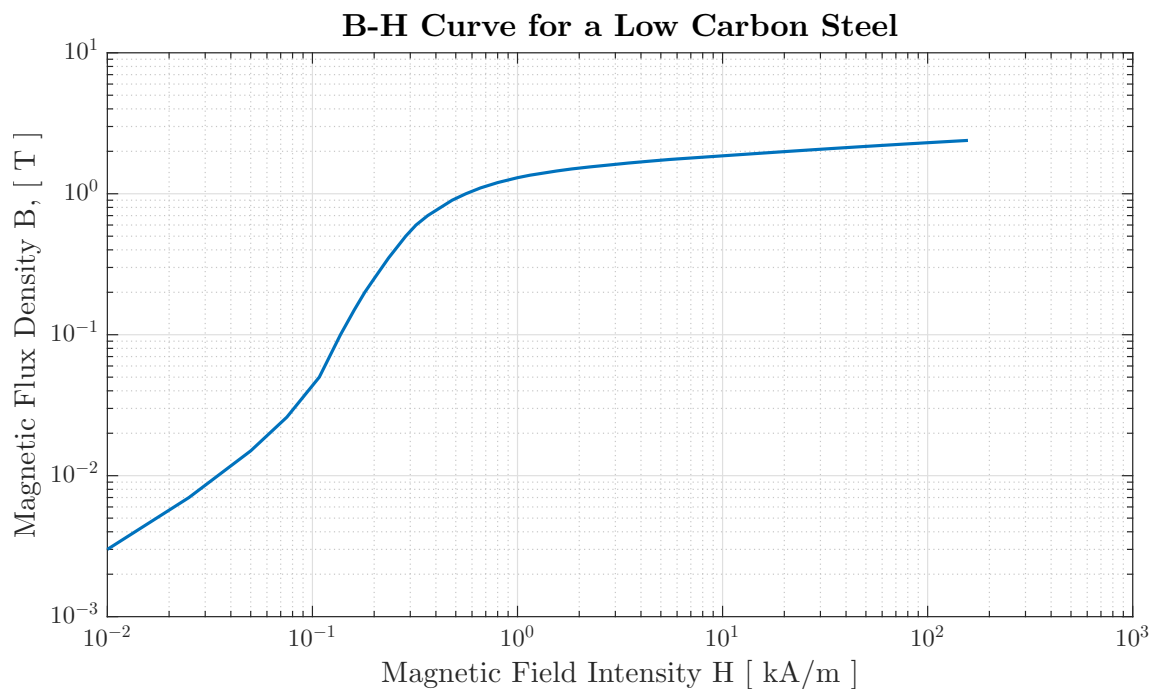


Figure 2.15: B-H Relation for low carbon steel. ([MagWeb, 2014](#))

2.4 CONCLUSION OF LITERATURE STUDY

A detailed overview of the $4S_4$ has been presented along with the characteristics associated with the $4S_4$. The first attempt to replace the solenoid valves with an MR valve done by [Meester](#) was also presented. Lastly all the necessary theory and concepts has been covered in order to design a new smaller valve.

CHAPTER 3

MAGNETO-RHEOLOGICAL (MR) VALVE DEVELOPMENT

This chapter describes the development of the first MR valve prototype in this dissertation. Section 3.1 outlines the design phase. Here the design requirements as well as the figures and values used during the design are outlined. Section 3.2 briefly describes the test setup used to characterise the valve. Section 3.3 discusses the results from the experimental tests as well as the final model used. Section 3.4 concludes this chapter with recommendations for design changes required to meet the initial specifications.

3.1 DESIGN

The purpose of this design is to develop a MR valve that is smaller than the one developed by Meeser. Therefore, the design requirements will be based on the $4S_4$. This means that the MR valve should be able to fit into the existing $4S_4$ valve block.

There are two major design requirements:

- The first is the ability to handle the required flow rates and pressure drops.
- The second is the size requirement.

Flow Requirements In order to aid with the design of the valve, Meeser took the optimized force-velocity curve (Thoresson et al., 2009) of the $4S_4$ suspension and converted it into a more convenient pressure drop *vs.* flow rate curve as shown in Figure 3.1.

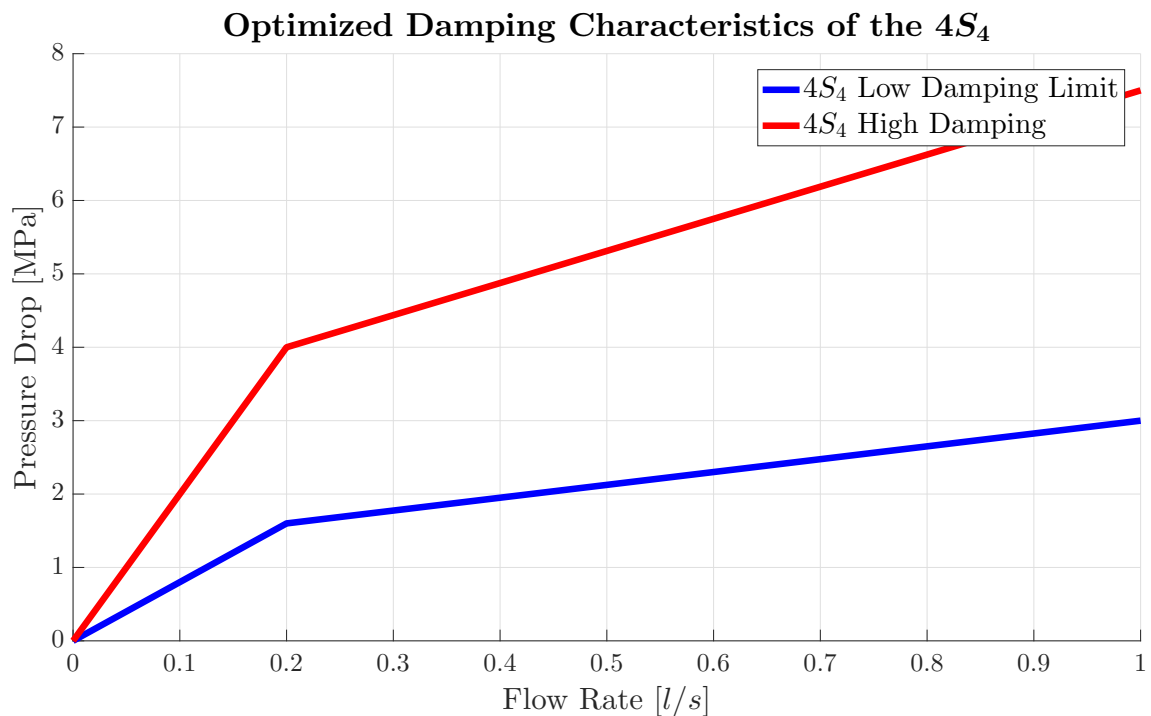


Figure 3.1: Optimised High and Low pressure drop *vs.* characteristics of the 4S₄. (Meeser, 2014)

For design purposes a maximum flow rate of $1l/s$ will be considered along with a maximum pressure of $10MPa$.

Size Envelope It is suggested that the size of the MR valve should not exceed a volume of $100 \times 100 \times 100mm$, so as to fit into the space envelope of the current 4S₄ valve block.

3.1.1 Properties and Figures used in the Design

For the purpose of replication all data that is used within the design will be listed in this section.

Fluid in Stock The MR fluid that will be used for the experiment is the MRHCCS4-B from Liquids Research (2014).

The fluid has the following properties:

Fluid Type	MRHCCS4-B
Density	3.18 g/ ml ($\pm 5\%$)
Viscosity @27C	Thixotropic
Saturation Magnetization	80%
Magnetically Active	80% by weight

Thixotropix: It is a shear thinning property. Certain fluids that are thick under static condition will flow over time when shaken, agitated, or otherwise stressed.

Assuming that the density of iron is 7.874 g/ml, the percentage iron particles by volume can be calculated as 32.3%. The value of 32% will however be used to correspond to the fluid properties described in the literature study.

Design Point Figure 3.2 shows the design point [$\mathbf{H} = 180 \text{ kA/m}$] for the magnetic circuit. The point is completely arbitrary, but the point was chosen not to be too high with the response time of the fluid in mind as well as that of the magnetic circuit. Because of the converging nature of the characteristic curve, more effort is required from the magnet to reach that point. The more effort that is require from the magnet the worse the response time will be.

Saturation An important concept that should be considered is the saturation limit of the MR fluid, because if the fluid is saturated no extra MR effect will be generated under a stronger magnetic field.

Jolly et al. (1999) says that the intrinsic induction of an MR fluid at complete saturation is ϕJ_s Tesla, where ϕ is the volume percentage of particles in the fluid and J_s is the saturation polarization of the particle material.

If the assumption is made that the particulate in the present MR fluid are made out of iron, $J_s = 2.1$ Tesla, then the MR fluid in stock will saturate at 0.672 Tesla. This value however is not to far below the chosen design point as seen in Figure 3.3 and will only slightly influence the response time of the valve. The magnetic circuit has an overbearing influence on the response time whereas the MR fluid will vary with a millisecond or two.

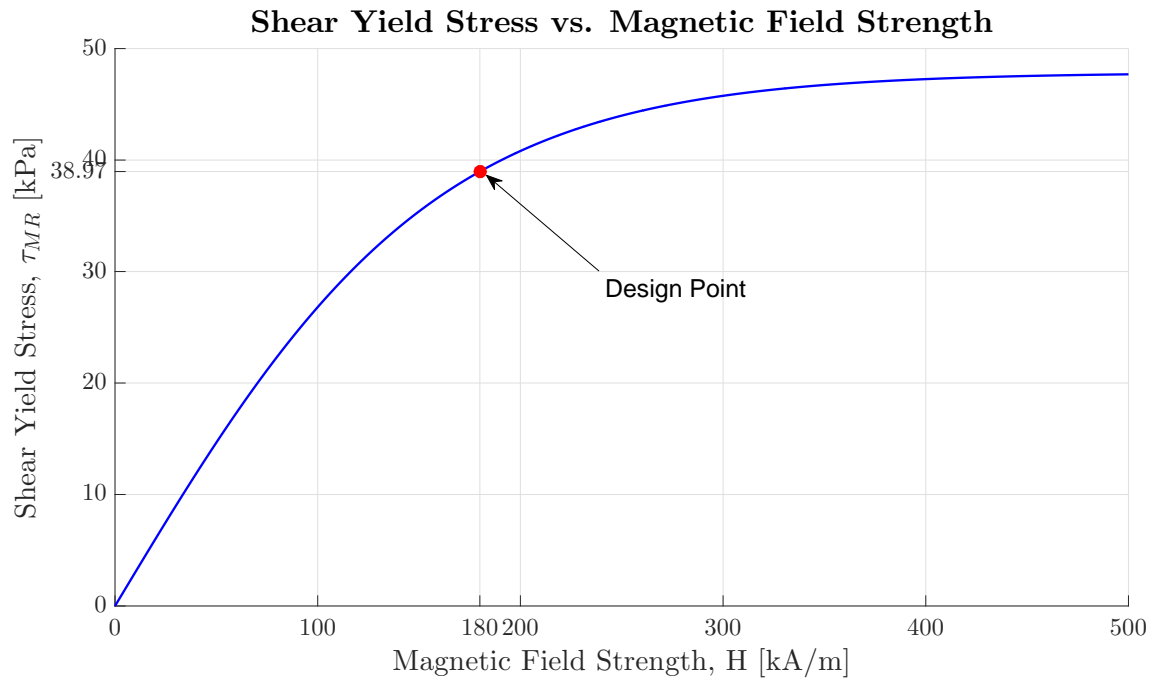


Figure 3.2: Design point for the magnetic circuit using [Equation 2.2](#)

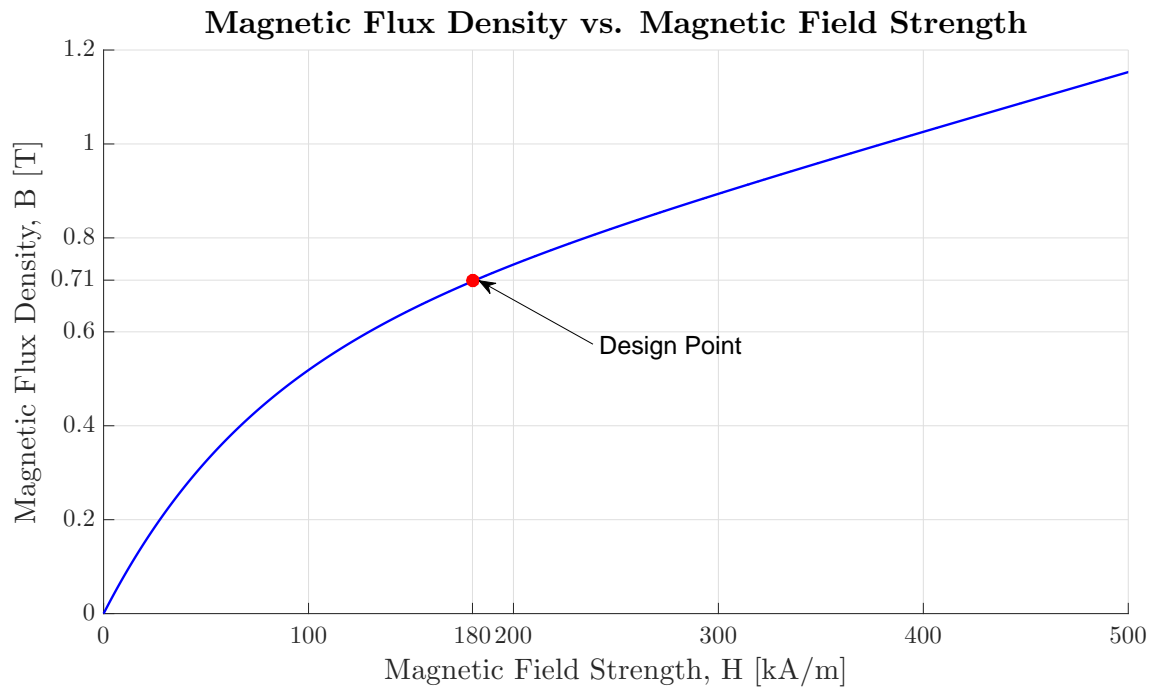


Figure 3.3: Design point according to fluid saturation.

3.1.2 Design of the annular flow area

The design of the prototype valve is based upon Equation 2.4 from Phillips (1969) rather than Equation 2.5 from Dixon (2007) which allows for a simplistic way to get a design without too many complications. An expression that will not be used is the minimum active volume relation (Equation 2.6) described in the literature, as it is only an algebraic manipulation of the design equation.

The equation that will be used for the present design is based on the flow between two parallel plates where the effects of the side walls are neglected, but since we are using an annular flow area with a small gap we would approximately get the same flow characteristics.

For convenience, Equation 2.4 is repeated here.

$$\Delta P = \Delta P_{\eta} + \Delta P_{\tau} = \frac{12\eta QL_1}{g^3 w} + \frac{c\tau_y(H)L_2}{g} \quad (3.1)$$

3.1.3 Design of the magnetic circuit

Magnetic field simulation was used as a method to determine the geometry of the magnetic circuit. Even though it would only be a rough estimate of the geometry the software allows for easy change of the geometry. The software that was used is an advanced nonlinear & multi-physics package from MSC (2014) called MARC Mentat.

Figure 3.4 shows the final geometry from the simulation as well as the approximate dimensions. In the simulation Figure 3.3 was used for the magnetic properties of the MR fluid and the B-H relation of a low carbon steel was also used in the simulation. For the properties of air as well as for the insulating materials (like the aluminium sections) μ_0 was used.

The results of this simulation shown in Figure 3.5 is in the form of the magnetic field intensity, H. This figure shows that the highest value of magnetic field density is right in the MR fluid gap. From these results we can see that the magnetic field H is in the region of 150 kA/m to 240 kA/m which is more than sufficient to achieve the desired MR effect. The design point in Figure 3.2 falls in this region.

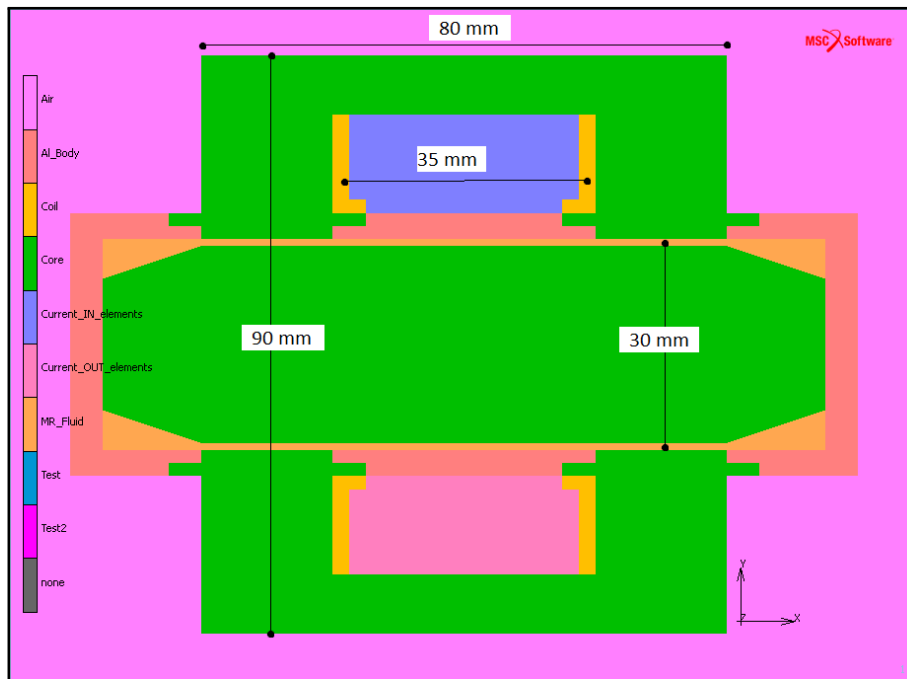


Figure 3.4: Geometry determined from the magnetic simulation.

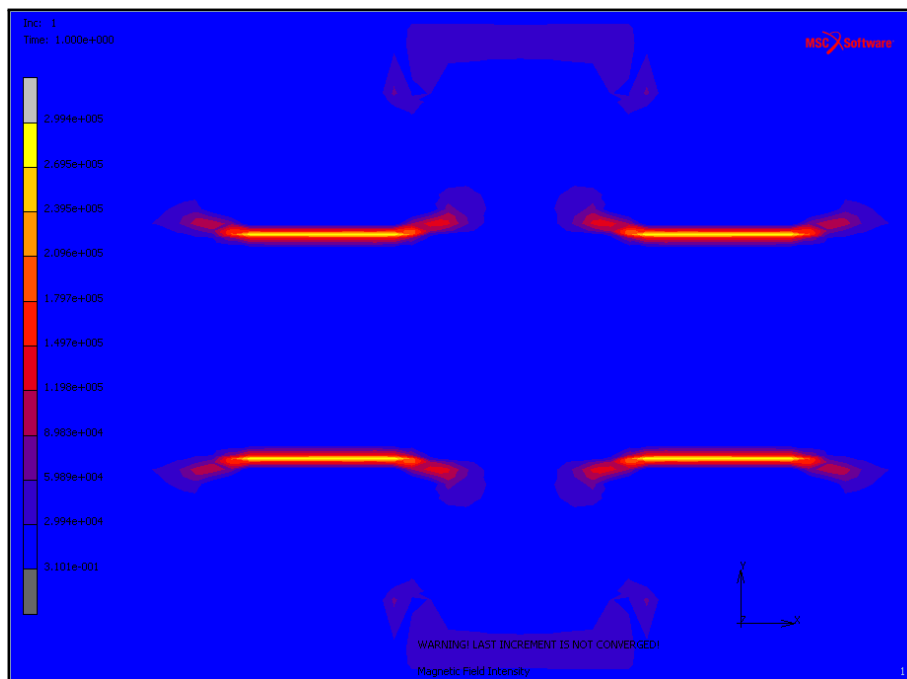


Figure 3.5: Simulation results for the magnetic field intensity H .

3.1.4 Final Design

Figure 3.6 shows the final geometry of the prototype valve that was manufactured.

The working principle of the current MR valve is exactly the same as the valve developed by Meeser. Both valves operate using the valve mode and utilize magnetic field lines perpendicular to the flow of fluid.

Figure 3.7 shows a section view of the current prototype. An annular flow area was chosen for this valve as this allows for a more compact design, but unfortunately increases the complexity of the magnetic circuit. The annular flow volume has a length of 90 mm, an outer diameter of 30 mm and a gap size of 1 mm as noted in Figure 3.6.

Part of the objective for this design was not only to achieve the same performance as the MR valve designed by Meeser, but also to reduce the size of the valve to make it practical. Figure 3.8 shows a size comparison of the MR valve by Meeser (left) and the current prototype (right). The second valve is significantly smaller and this is attributed to the fact that the magnetic circuit surrounds the valve which significantly reduces the size.

3.2 TEST SETUP

Figure 3.9 shows the test set-up with (1) a 100 kN Shenck servo hydraulic actuator, (2) a 100 kN load cell, (3) a double acting hydraulic cylinder and (4) the prototype MR valve with pressure transducers (A and B).

The double acting hydraulic cylinder has a piston diameter of 70 mm and a rod diameter of 35 mm. Using these dimensions, it is possible to convert the flow rate in the cylinder to piston velocity, which is also the actuator velocity. This is only an approximation as the fluid compressibility was not considered.

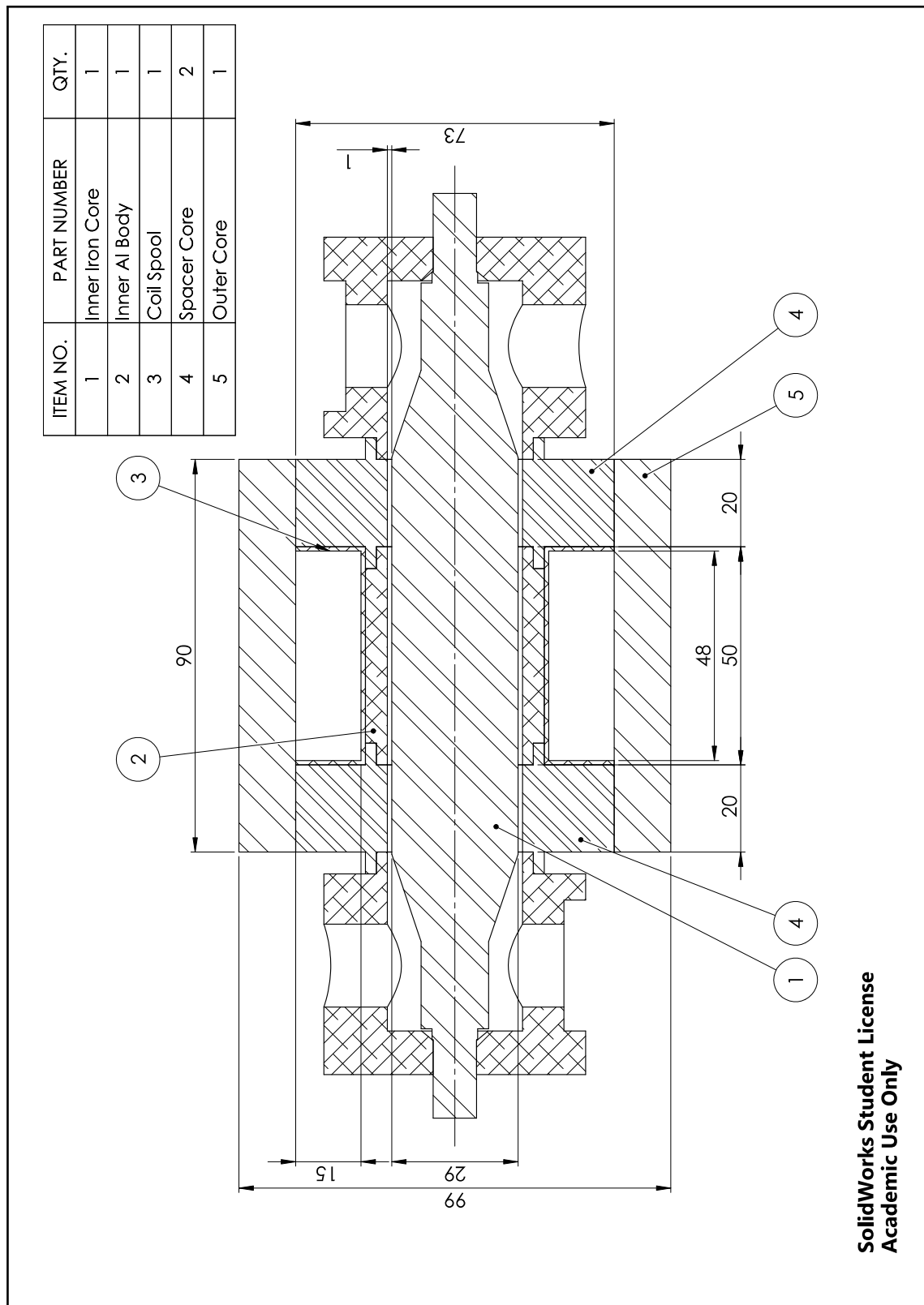


Figure 3.6: Final Geometry of the prototype MR valve

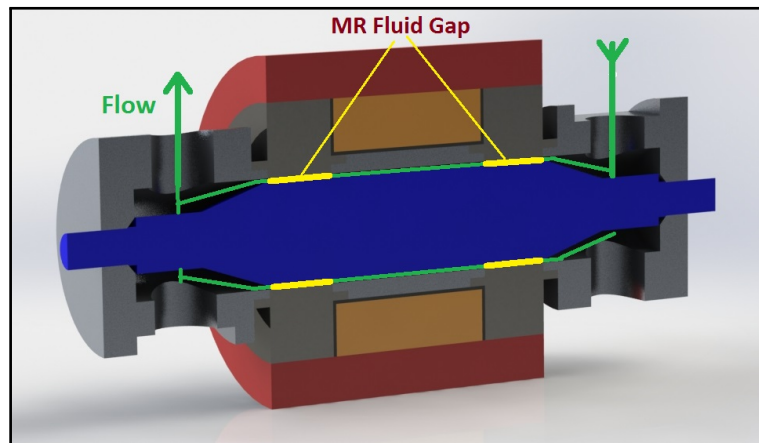


Figure 3.7: MR Valve showing MR Fluid Flow and MR Gap



Figure 3.8: Size comparison between the MR valve by Meeser (Left) and the current prototype (Right)

3.3 RESULTS

3.3.1 Flow Blocking

Figure 3.10 shows the results of the flow blocking tests performed on the MR valve. An extremely low flow rate achieves a blocking force just around 4 kN, the same as Meeser (2014). This extremely low flow rate results in a $4S_4$ strut velocity of approximately 0.0007 m/s. This means that in a period of 10 s the suspension will only move 7 mm.

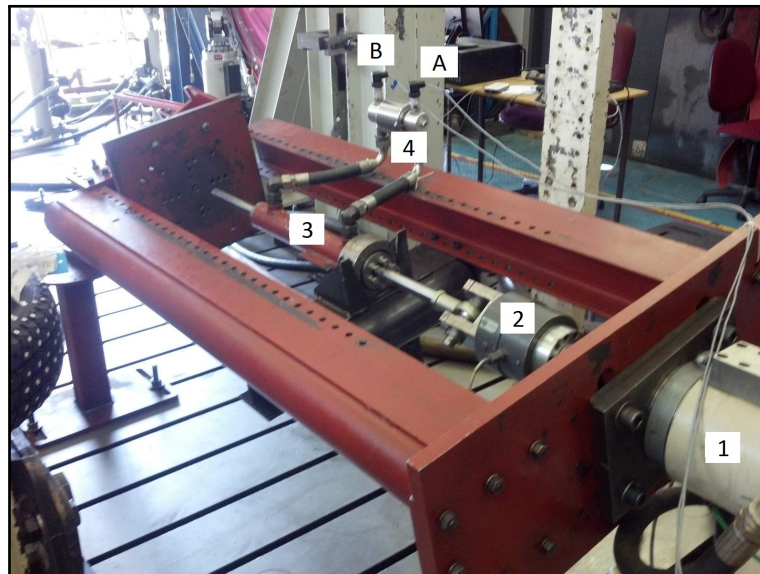


Figure 3.9: The test setup showing the red frame and double acting piston.

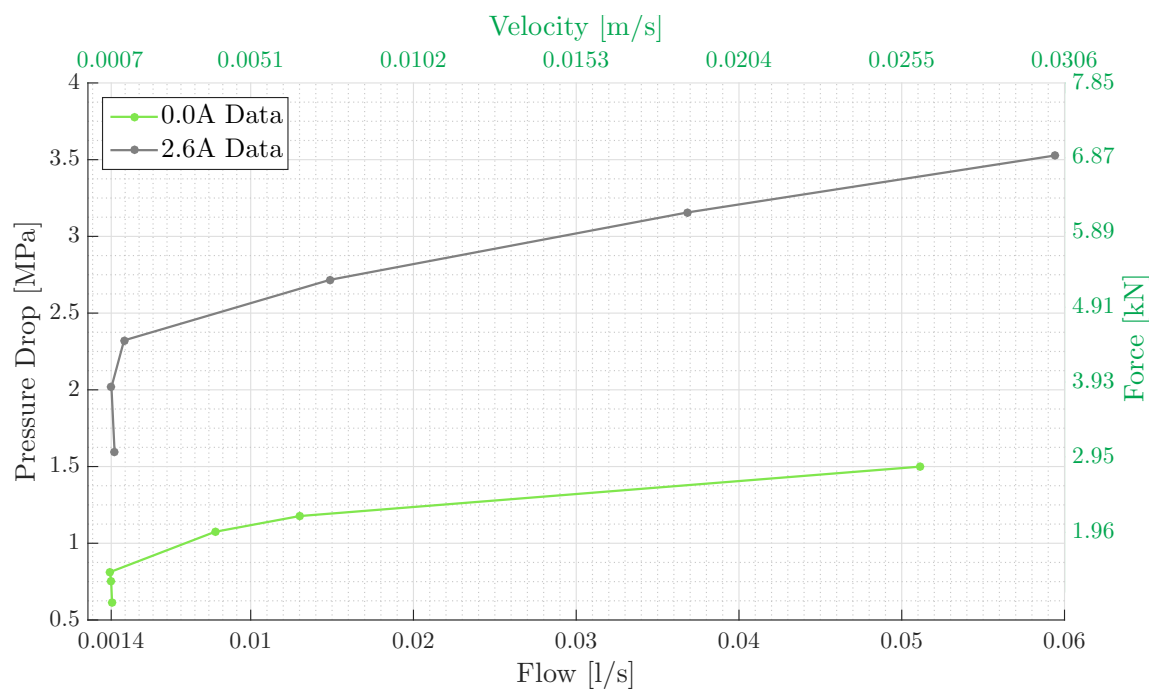


Figure 3.10: Experimental results obtained from the Flow Blocking tests.

3.3.2 Damping

Figure 3.12 shows the Force-Velocity curve of the current valve prototype along with the upper and lower limits of the optimised $4S_4$ characteristics and the flow blocking data from

Figure 3.10. From the figure it is clear that current valve characteristics exceeds the lower limit of the $4S_4$ characteristics. It is also seen that for the lower flow rates the damping force is much higher than those reported by Meeser in Figure 2.9. This is due to the thixotropic (shear thinning) property of the MR fluid which suggests that Meeser did not account for shear thinning in his model in the off-state.

3.3.3 Theoretical Model

The fluid viscosity in the absence of a magnetic field is most significantly a function of the carrier oil, suspension agents, and particle loading. Because of both the addition of suspension agents and changes in magnetic particle micro structure during shear, most MR fluids exhibit significant shear thinning. (Jolly et al., 1999)

In order to include the thixotropic (shear thinning) property of the MR fluid into theoretical model, the viscosity must first be described a function of shear rate.

Therefore keeping with the notation of Figure 2.14 the shear rate is determined by

$$\dot{\gamma} = \frac{6Q}{wg^2} \quad (3.2)$$

The shear thinning property causes a decrease in viscosity with increase in fluid shear rate, it is therefore important to know the viscosity of the MR fluid as a function of the shear stress or shear rate. In order to describe the viscosity as a function of shear rate, the following power law relation is suggested

$$\eta = a(p \cdot \dot{\gamma})^{-k} \quad (3.3)$$

where a is a function of temperature, p is a scaling factor and k is the power law constant.

Fluid Model Consider Figure 3.11, notice how the data for the **2.6A** valve current (on-state) isn't just a vertical shift as suggested by Equation 2.4. Instead, the pressure drop is less than expected at lower flow rates. For this reason a small modifying function were introduced. The model, as a function of shear rate, is as follows

$$f(\dot{\gamma}) = \frac{1}{2}(2 - e^{-q \cdot \dot{\gamma}}) \quad (3.4)$$

where q is also just a scaling factor.

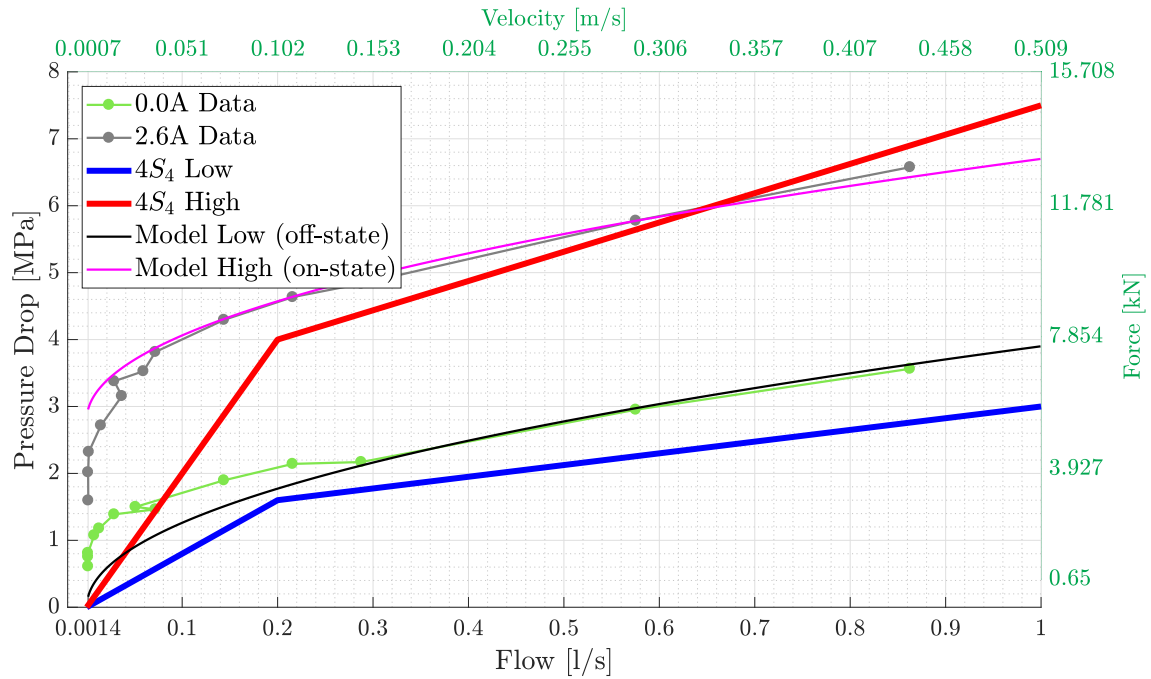


Figure 3.11: Combined Damping and Flow Blocking Results with the original theoretical model for the off-state.

Utilizing the viscosity (Equation 3.3) together with the modifying function (Equation 3.4) as a function of shear rate (Equation 3.2), the relation for pressure drop across a valve as a function of flow rate and apparent fluid shear stress (Equation 2.4) can be rewritten as follows

$$\Delta P = \Delta P_{\eta} + \Delta P_{\tau} = \frac{12\eta(\dot{\gamma})QL}{g^3w} + \frac{c\tau_y(H)L_c}{g} \cdot f(\dot{\gamma}) \quad (3.5)$$

Figure 3.12 shows the fitted theoretical model and Table 3.1 gives the values of the constants used in Equation 3.5. The table also provides a summary of the valve geometry, or rather the annular flow volume.

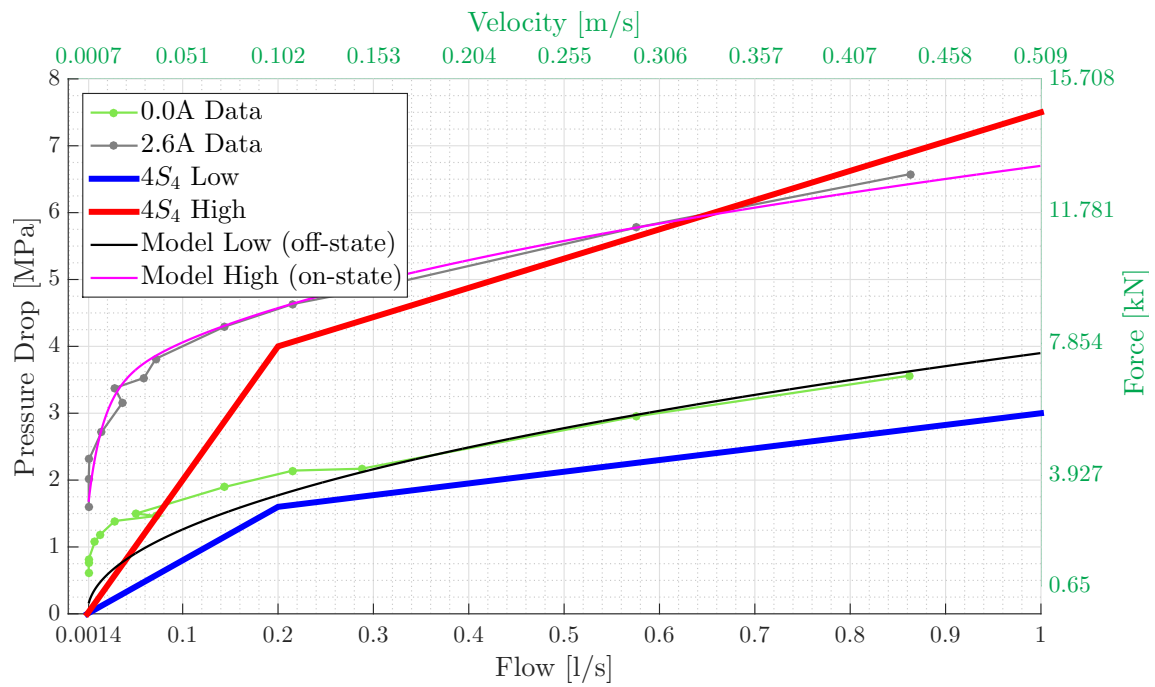


Figure 3.12: Combined Damping and Flow Blocking Results with the adjusted theoretical model for the off-state.

Table 3.1: Values of the constants used in Equation 3.3, Equation 3.4 and Equation 3.5

a	1
p	$1.3e(-4)$
k	0.51
q	$1.0e(-3)$
L	90mm
w	$30\pi mm$
g	1mm
c	2
τ_y (on-state)	35kPa

3.3.4 Response Time

As mentioned previously the response time of the solenoid valves in the 4S₄ is in the region of **40-100 ms** (for a **5-95%** response time value). The response time of the current valve was measured to be in the region of **40 ms** (for the well known **63.2%** response time). This

indicates that the current valve response time is far worse and that these two values cannot be directly compared. The response time were determined by measuring the voltage over the coil as the circuit is activated over time. Therefore, the value has no meaning.

3.4 PROPOSED DESIGN AMENDMENTS

As seen in Figure 3.12 the current valve exceeds the lower optimised limit of the $4S_4$. Figure 3.13 shows simulation of the new proposed valve characteristics for a larger gap size of 1.2 mm. The trade-off here is the reduced MR effect due to the larger gap size. However, this reduced MR effect is based on the fact that the magnetic field within the fluid will cause the same shear stress. With a more effective magnetic circuit the MR effect can be increased.

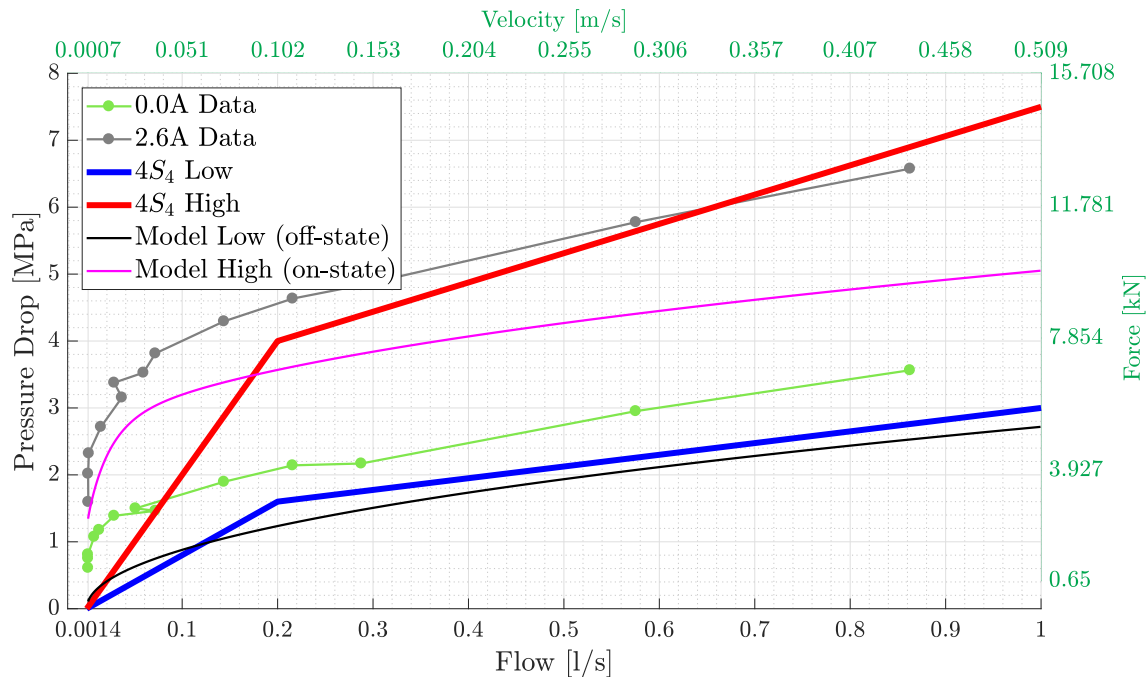


Figure 3.13: Valve Characteristics due to larger 1.2 mm gap size.

The research presented here have shown that with a simple prototype it is possible to build a smaller magneto-rheological (MR) valve than the one Meeser built, while still achieving the same damping range and flow blocking capabilities. The results presented here warranted another prototype as will be described in the next chapter.

CHAPTER 4

MAGNETO-RHEOLOGICAL (MR) $4S_4$ DEVELOPMENT

Based on the feasibility of the MR valve developed in chapter 3, two of these valves are now implemented to form a MR $4S_4$. The geometry of the previous design is used as a starting point refined to include the recommended improvements.

Section 4.1 describes the design of the magnetic circuit using a more analytical approach. Section 4.2 provides a description of the final modified $4S_4$ and all the sensors used as well as the experimental setup, followed by a summary in Section 4.3.

4.1 MAGNET DESIGN

For the current design an analytical approach was rather used to determine the geometry compared to the FEM based approach used in Chapter 3. The first prototype MR valve presented in Chapter 3 made use of EN24 steel, which was readily available at the time. This led to inaccuracies in the design of magnetic circuit because the magnetic properties of metal had to be estimated. For the MR valve presented in this chapter it was decided to use a low carbon steel, EN3A, as the magnetic material as it can be considered as a "soft iron". [Figure 2.15](#) gives the BH relation for low carbon steel.

4.1.1 Magnetic Circuit

[Figure 4.1](#) shows a cross section of the magnetic circuit for the magneto-rheological (MR) valve used in this study,

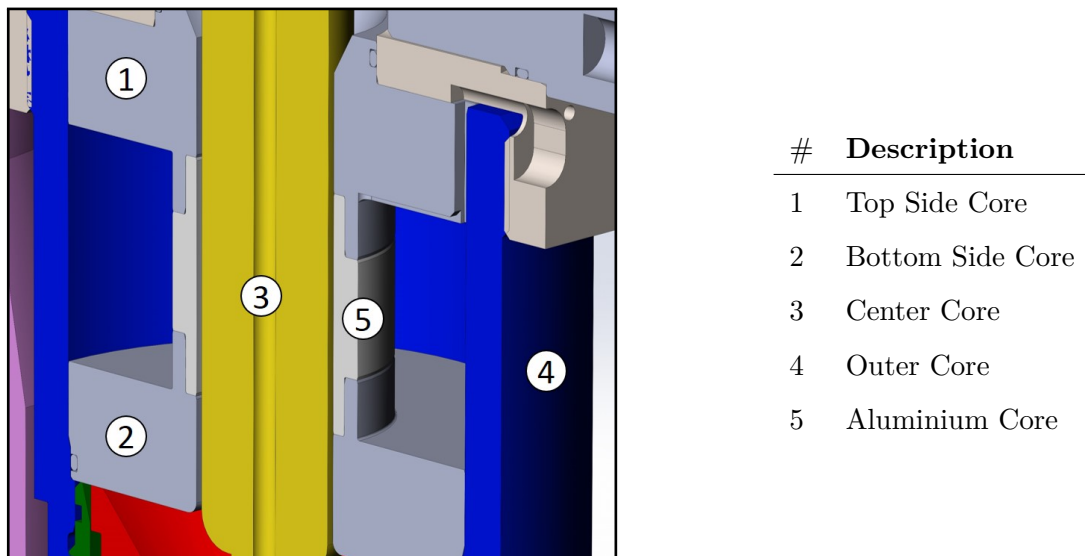


Figure 4.1: Elements of the magnetic circuit.

Figure 4.1 indicates only the solid elements of the magnetic circuit. The remaining element, and also the most important, is the MR fluid. The MR fluid fills the annulus between elements 1-3, 5-3 and 2-3. The so called *MR effect* is developed in the annulus between elements 1-3 and 2-3 which are known as the **MR gaps**. The purpose of the aluminium core in the circuit is to act as an insulator. This forces the magnetic flux through the **MR gaps**.

4.1.2 Magnetic-Electric Circuit Analogy

Figure 4.2 shows the analogous electric circuit for the MR valve. The resistors represent the different magnetic elements with the numbering according to that of Figure 4.1. The battery is analogous to the coil, which provides the magneto motive force (MMF) that drives the flow of magnetic flux in the circuit.

4.1.3 Solution

Using this simplified analytical model for the magnetic circuit it is possible to solve for the circuit in steps. The design point, or rather where the solution originates from is the magnetic field strength in the MR fluid gap (which is $H = 180kA/m$ as determined in Chapter 3).

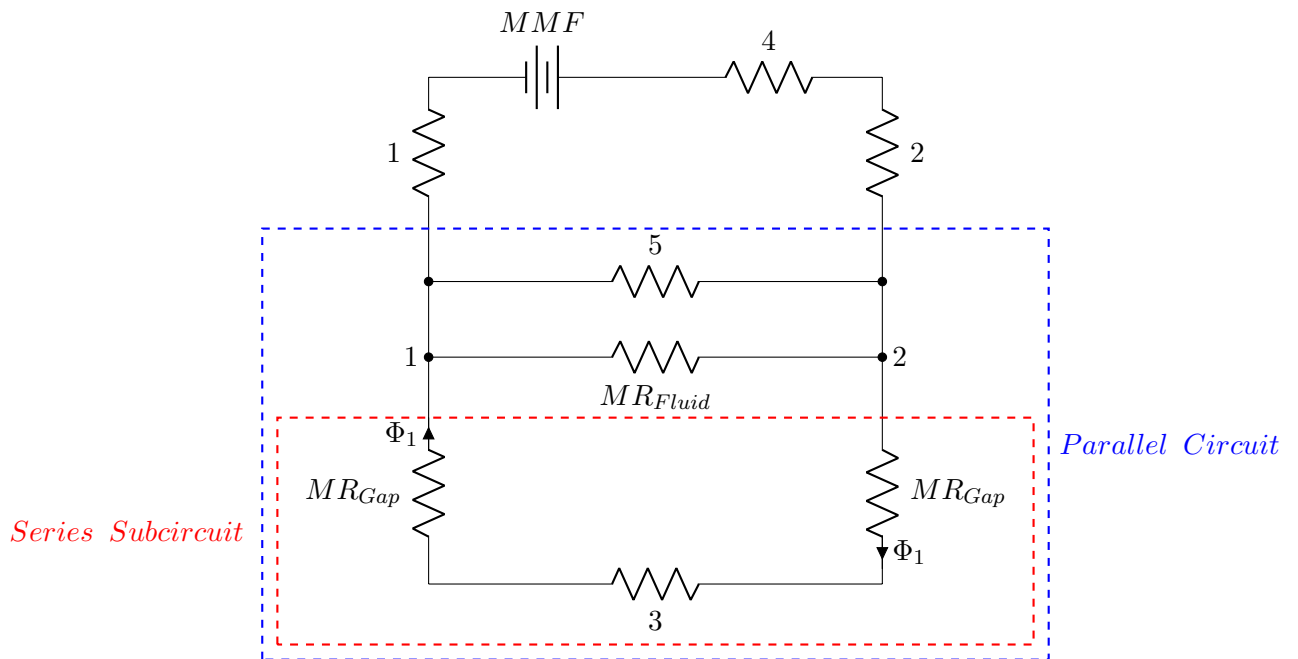


Figure 4.2: Analogous electric circuit for the MR valve.

Series Sub-Circuit

Knowing the required magnetic field in the MR fluid gap, the geometry along with the MR B-H curve can be used to determine the magnetic flux, Φ_1 , flowing through the MR fluid gap and the reluctance, \mathcal{R} , of each gap. Once the Φ_1 value through the elements are known it is possible to calculate the \mathcal{R}_{series} of the circuit and finally the MMF .

Parallel Sub-Circuit

Now that the magneto motive force over nodes 1-2 are known, which is also the MMF over the parallel circuit, the reluctances of the MR_{Fluid} and aluminium core can be determined using the already predefined geometry. The $\mathcal{R}_{parallel}$ can be determined and the magnetic flux, $\Phi_{parallel}$, through the parallel circuit can be calculated.

Remaining Elements

The sizes for the outer core as well as the two side cores can be calculated using the magnetic flux. This process is iterative due to the fact that the coil is enclosed between the outer core,

side cores and the aluminium core. A brute-force method is used by just gradually increasing the diameters of the side cores. At each diameter the approximate number of turns in the coil is also calculated along with the resistance of the coil and finally the magneto motive force. This process is repeated until an appropriate combination is found.

4.2 EXPERIMENTAL SET-UP

For the test setup, the same red frame as seen in [Figure 3.9](#) was used to hold the suspension in position. In total 28 analogue channels were recorded as described in [subsection 4.2.1](#).

4.2.1 Sensor Descriptions

[Figure 4.3](#) shows the locations and numbers of the main sensors used in this study. The different sensors at the indicated locations are described in the table below:

Location	Description
1	Temperature and pressure measurement in fluid chamber located near the main strut.
2	Temperature and pressure measurement of large accumulator gas chamber.
3	Temperature and pressure measurement of fluid chamber between the floating piston and MR valve exit in large accumulator.
4	Temperature and pressure measurement of fluid chamber directly linked to main strut chamber, but as close as possible to the MR valve inlet on the side of the large accumulator.
5	Temperature and pressure measurement of small accumulator gas chamber.
6	Temperature and pressure measurement of fluid chamber between the floating piston and MR valve exit in small accumulator.
7	Temperature and pressure measurement of fluid chamber directly linked to main strut chamber, but as close as possible to the MR valve inlet on the side of the small accumulator.
8	Linear displacement sensor specifically designed to work in contact with hydraulic fluid.

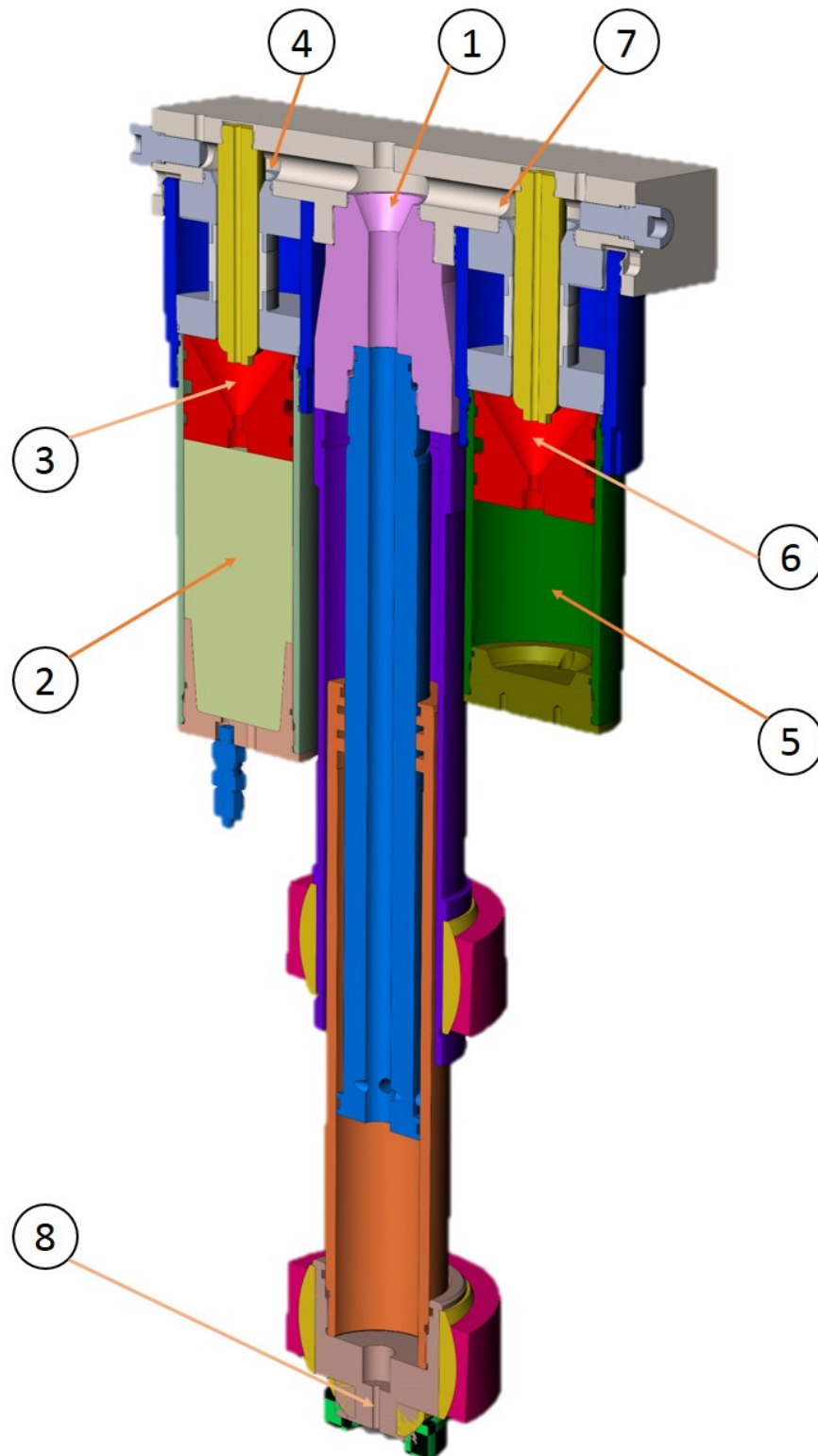


Figure 4.3: Numbering and Locations of the sensors used on the suspension during testing.

Additional sensors on the servo hydraulic Schenk Hydropulse actuator measure actual displacement and force. Current sensors on the coils for the MR valves as well as support sensors that measure the control signals, are also present. The temperature data is not used in this report, but gathered for future use.

4.2.2 Pressure Measurement based on Thin Pressure Vessel Theory

Rugged pressure transducers are quite expensive, whereas strain gauges are cheap and easily replaceable in comparison. The biggest asset in a control system is feedback. An increase in the available feedback allows for better and more precise control. By having strain gauges that is permanently mounted on the suspension at key locations makes it easier to control for example the MR valves to get the desired suspension characteristics.

It was suggested by [Els \(2006\)](#) to measure both the fluid and the gas pressures in the accumulators using strain gauges. This is related to the thin walled pressure vessel theory, since the strain measure on the outer surface is proportional to the pressure inside the vessel.

It was necessary to rework the current accumulators as the wall thickness was too large. Therefore using the thin walled pressure vessel theory the appropriate reduction in outer diameter was determined as is shown in [Figure 4.4](#).

[Figure 4.5](#) shows the results of FEM analysis that was done using Ansys. The purpose of the analysis was to determine whether the reduced diameter sections on the accumulator was long enough so that approximately uniform stress and strain would be measured by the strain gauges.

4.3 CONCLUSION

In this section the design of the magnetic circuit for the new MR valve as well as the process to solve for the magnetic elements and coil using and analytical method was described. The magnet design was based on the results obtained in chapter 3.

Furthermore, the proposed use of thin walled pressure vessel theory to determine the pressures of the fluid and gas in the accumulators were also described. Next the details of the new prototype as well as the integration of the MR valves into system were presented

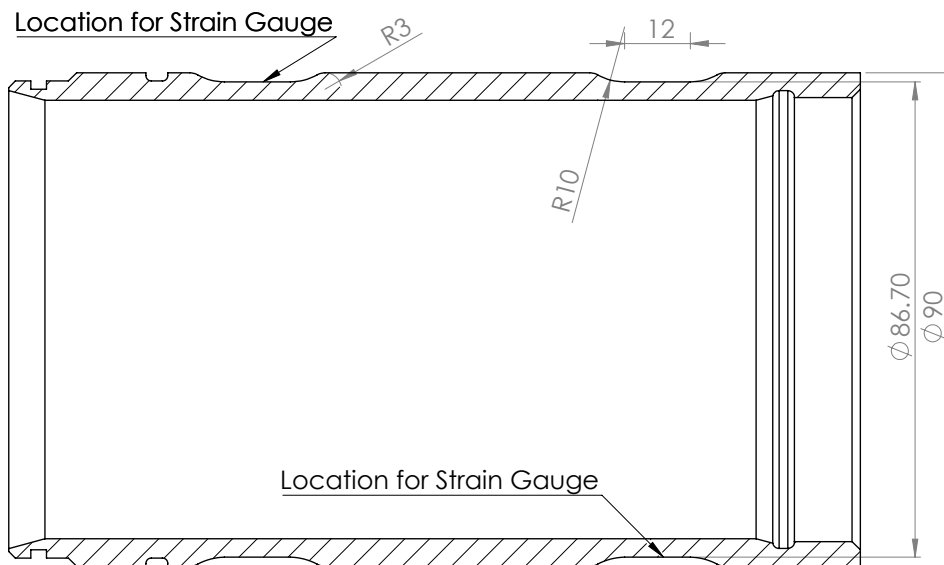
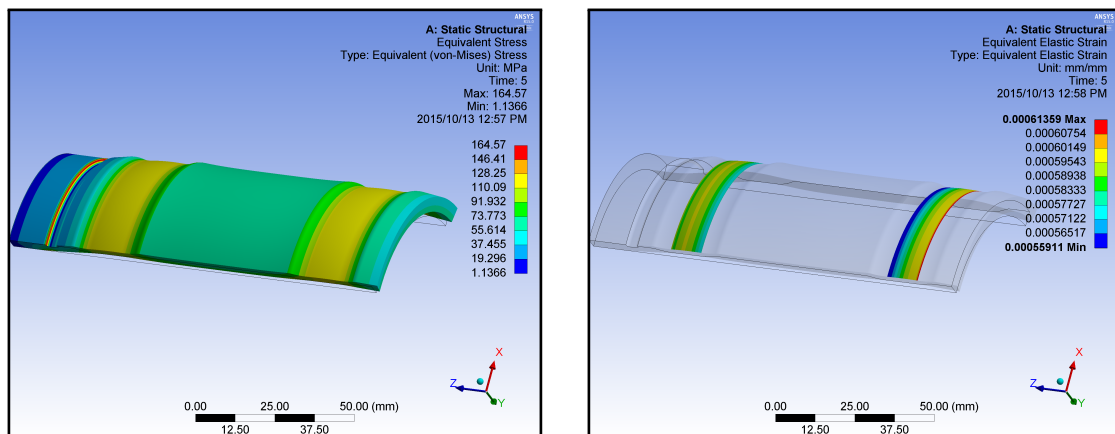


Figure 4.4: Cross section of the accumulator sleeve showing the turned down sections where the strain gauges will be placed.



(a) Total Stress in the turned down regions

(b) Strain in the turned down regions

Figure 4.5: Results of a FEM analysis to determine whether the turned down sections are long enough for uniform stress/strain.

Finally the test setup including the sensors used, their locations, and data acquisition system were described.

CHAPTER 5

RESULTS

This chapter presents processed results and insights obtained from the experimental testing. Contained within this chapter is the results for the bulk modulus (Section 5.1) of the fluid, which was tested before the gas accumulators were charged; the response time (Section 5.2) details of the $4S_4$ system during dynamic tests as well as that of the magnets; three different spring rates (Section 5.3); the flow blocking (Section 5.4) ability of the MR valves crucial to be able to switch between spring rates; the damping (Section 5.5) results along with some extra findings from the damping data and finally the results from the strain gauges installed on the accumulators.

Removing noise from data Testing was conducted in an environment where multiple other tests and experiments were conducted. This added a considerable amount of noise to the recorded data. To remove the noise, the upper and lower band of the data was determined, the mean was calculated and taken as the cleaner data as shown in [Figure 5.1](#). Frequency based filters were first implemented but either distorted a clearly visible trend in the data or left the data too noisy.

Calibrating the current The current of both valves was measured using the current sense pin on a FAN7093 H-Bridge driver. The measured values was calibrated using the values written down from the dual channel power supply. As an added measure, the control signal was also measured on the input pins of the FAN7093 drivers. This was used to verify that an increase in current coincides with the control signal given by the data acquisition system.

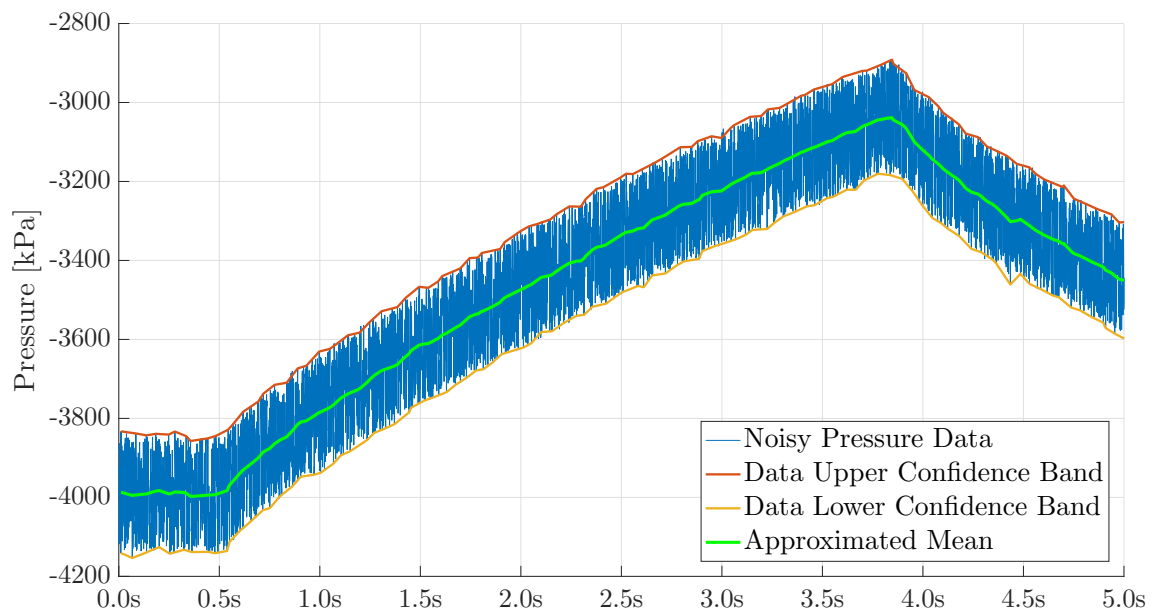


Figure 5.1: Method used to clean the data.

5.1 BULK MODULUS

To determine the bulk modulus, the floating pistons needed to reach their respective bottom stops in the accumulators while exposed to atmospheric pressure. This was achieved by continuously filling and compressing the main strut. The process is complete when the main strut is at a retracted position from full compression and a large increase in the measured force is registered. The main strut is then slowly compressed and decompressed for a few cycles. The stroke of these cycles are quite small because a small amount of compression produces a large increase in measured force.

[Figure 5.2](#) shows the data from the pressure sensors in the 5 different MR fluid locations. As expected they correlate well with each other. It is seen that for the first 4 mm (-110 mm to -114 mm) the data is not in line with the rest of the stroke. This can be the cause of "play" and stiffness in the test rig and the fact that the pistons are not completely bottomed out.

A straight line was fitted to the data in [Figure 5.2](#) to obtain a Bulk Modulus of approximately 1.6 GPa/m .

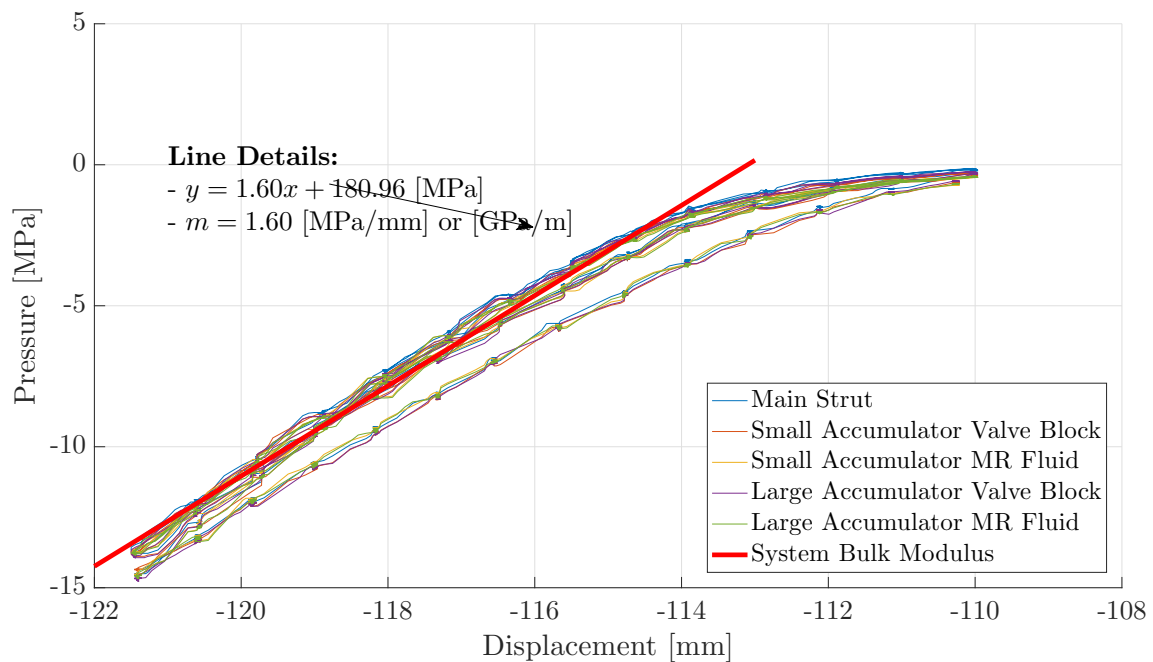


Figure 5.2: Pressure-Displacement Data of the Bulk Modulus measurement.

5.2 RESPONSE TIME

During the tests, a dual channel variable power supply was used to energize the coils of the two valves. This power supply was also used during the response time tests, but due to concerns that the power supply would introduce extra delays in the response time measurements, the tests were repeated using a 12V lead acid battery as well. However, after analysis of the data it was discovered that there was a fault with the control circuit and that the coils were never energized by the battery. The battery tests were therefore not useful.

It was therefore decided to perform bench tests on the magnetic circuit using both the power supply and battery to determine whether the time response data from the power supply was indeed usable.

Measurement Method Figure 5.3 shows the circuit diagram that was used during the bench tests. On the diagram V_1 and V_3 measures the battery and coil voltages respectively. V_4 measures the input voltage to the MOSFET gate (control signal). ΔV_2 measures the voltage over the small high precision current sense resistor. The data acquisition system (see ??) was set to a sampling frequency of **10kHz** for these tests.

The response time was calculated at the commonly accepted **63.2%** point as well as the **5-95%** measure that was used by [Els \(2006\)](#) as shown in [Figure 5.4](#).

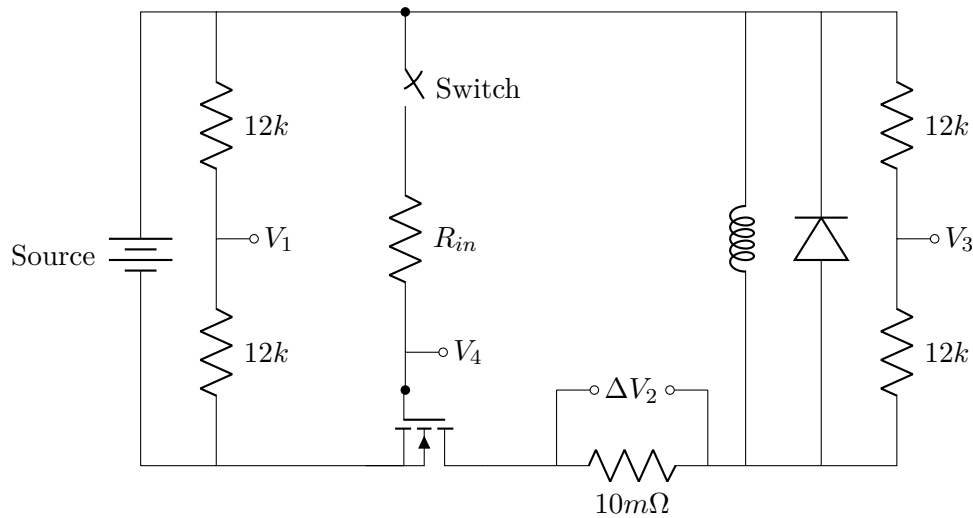


Figure 5.3: Control Circuit used to measure the magnetic circuit response time.

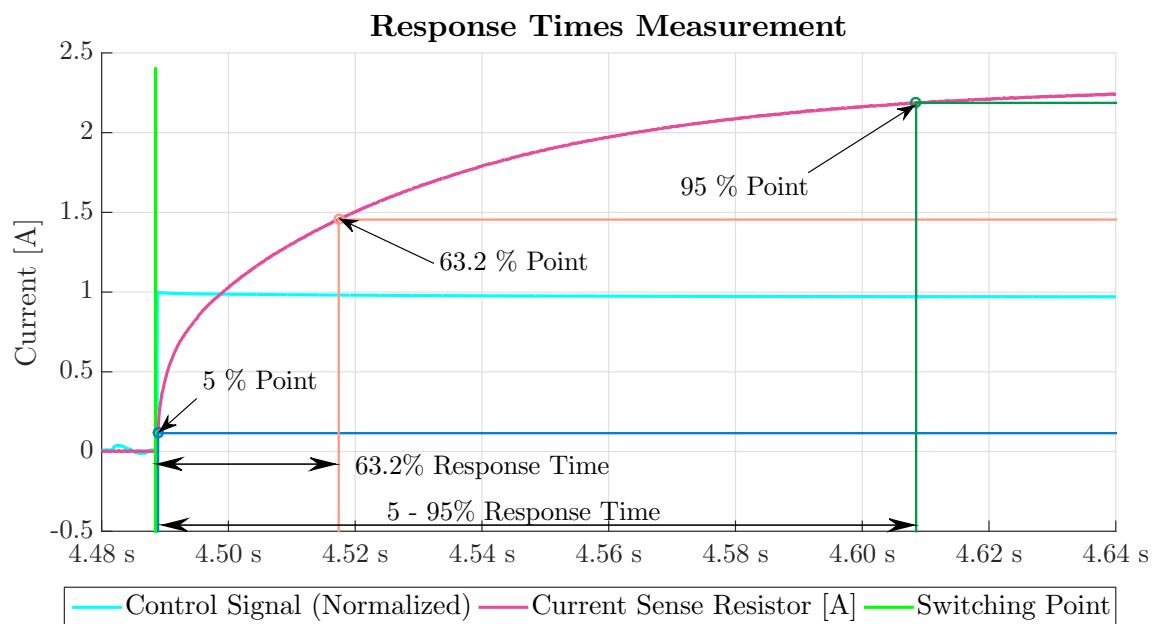


Figure 5.4: Typical measure during the time response tests.

[Table 5.1](#) shows the response times that were measured during the bench tests using both the battery and power supply. For the response time tests using the battery three scenarios were tested. The first is the magnet (see [Figure 4.1](#)) with no central core (Item 3 in [Figure 4.1](#)) and no MR fluid present. The second is the magnet with no MR fluid present but with the central core re-installed. The third is the magnet response time with MR fluid added to the

magnetic circuit. The table provides the average values of the supply voltage and response time taken over a number of measurements. From the results presented in the table (see lines 3 - 4) it was concluded that system response time measured using the dual power supply would be acceptable.

Table 5.1: Magnet Response Times

		Measure- ments	Supply Voltage [V]	Response Times [<i>ms</i>]	
				63.2% Time	5 - 95% Time
Response times with battery					
1	NO MR Fluid and NO CORE	20	12.22	7.4	25
2	NO MR Fluid	10	12.3	25	107
3	With MR Fluid	16	12.26	29	120
Response times with power supply					
4	With MR Fluid	11	12.25	29	119
5	With MR Fluid	6	18.8	28	106

From these measured values it can be stated that the addition of the central core (Line 2 in table) to the circuit increase the response time significantly whereas the addition of the MR fluid (Line 3 in table) does not increase the response time by the same magnitude. For the common 62.2% measurement the MR fluid only adds a few ms during static tests.

5.2.1 System Response Time

The system response time is a measurement of the time required for the system to develop maximum resistive force while fluid is forced through the valve.

To determine the system response time the force measured on the main strut was used. Firstly a data segment of the test was extracted, as shown in [Figure 5.5 \(a\)](#), which includes the moment before and after activation of the magnets. Secondly the data was de-trended using a fitted line and mirrored as shown in [\(b\)](#).

[Table 5.2](#) shows the results of the system response time measurements. The results however are only for a single slow suspension velocity of approximately 25mm/s . Even though the

response time of the magnet will not change, it is expected that the response time of the system will change along with the suspension velocity as was shown by Els (2006).

System Response (@0.025m/s)
 Small Accumulator Coil = 2.0 A
 Large Accumulator Coil = 2.0 A

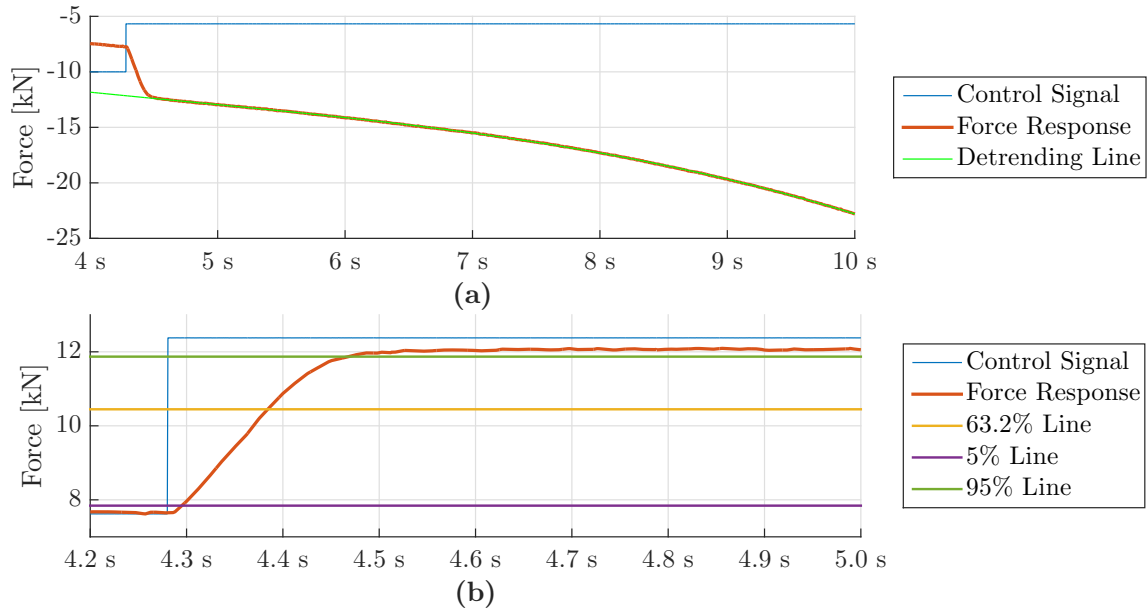


Figure 5.5: System response measurements using the force as measured on the main strut. (Magnets set to 2A each)

Table 5.2: System Response Times using the Power Supply

		Measure-ments	Supply Voltage [V]	Response Times [ms]	
				63.2% Time	5 - 95% Time
1	System Response	2	12.00	105	184

The system response time values in Table 5.2 are not desirable. The 5 - 95 % response time is more than double the 40 - 90ms response time reported by Els. This is a cause for concern as the desired response time is less than 40 ms. Based on the static response time measurements an improvement in the magnetic circuit (focusing on the central core) should improve the response time. However, a significant improvement in the dynamics response time is also required. Ex. a reduction in the MR gap thickness should prove favorable for the dynamic response since the dynamic response is not only a function of the magnetic circuit but also the geometry.

5.3 MR 4S₄ SPRING CHARACTERISTICS

The spring rates of the MR 4S₄ Suspension were determined by slowly compressing and decompressing the strut. A triangular input was used, but the displacement was done via discrete steps in time rather than a continuous motion. Each step allows the system to near equilibrium so as to cancel the effect of any damping.

5.3.1 Results for Soft Spring Setting

Figure 5.6 (c) presents the soft spring characteristic of the 4S₄ system determined from one full cycle of the strut. Figure 5.6 (a) & (b) show the measured strut displacement and measured force data respectively.

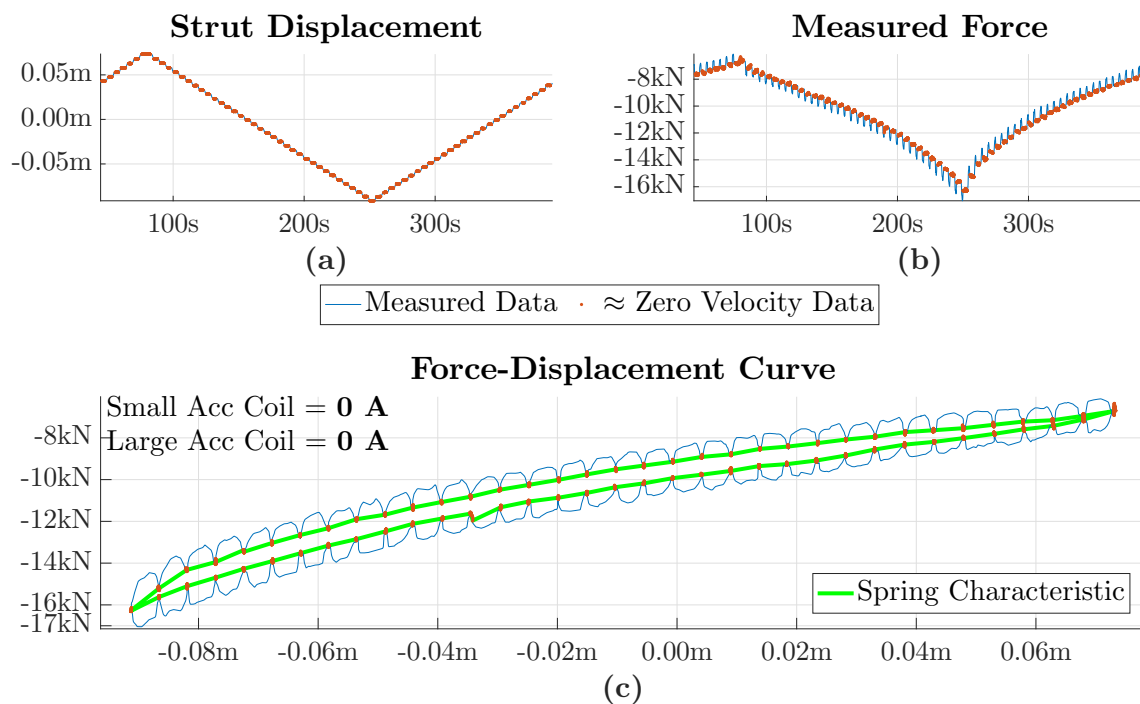


Figure 5.6: MR 4S₄ Soft spring curve.

5.3.2 Results for the first Hard Spring Setting

Figure 5.7 (c) shows the characteristic of the first hard spring setting on the MR 4S₄. The setting is characterised by the active coil which in this case is the coil located on the small accumulator side. Again, Figure 5.7 (a) & (b) shows the details of the measured strut

displacement and force data.

By having the coil of the smaller accumulator active the idea is to block the flow of fluid to the smaller accumulator and force all the fluid through the MR valve located at the on the side of the large accumulator. The ideal situation is where the gas in the small accumulator remains at constant pressure while the gas in the large accumulator is compressed and decompressed effectively changing the spring rate of the system.

Looking at the curve for the first hard spring setting, it can be seen that the hysteresis is smaller than that of Figure 5.6 which is a results of less moving components, *i.e.* one less floating piston with friction.

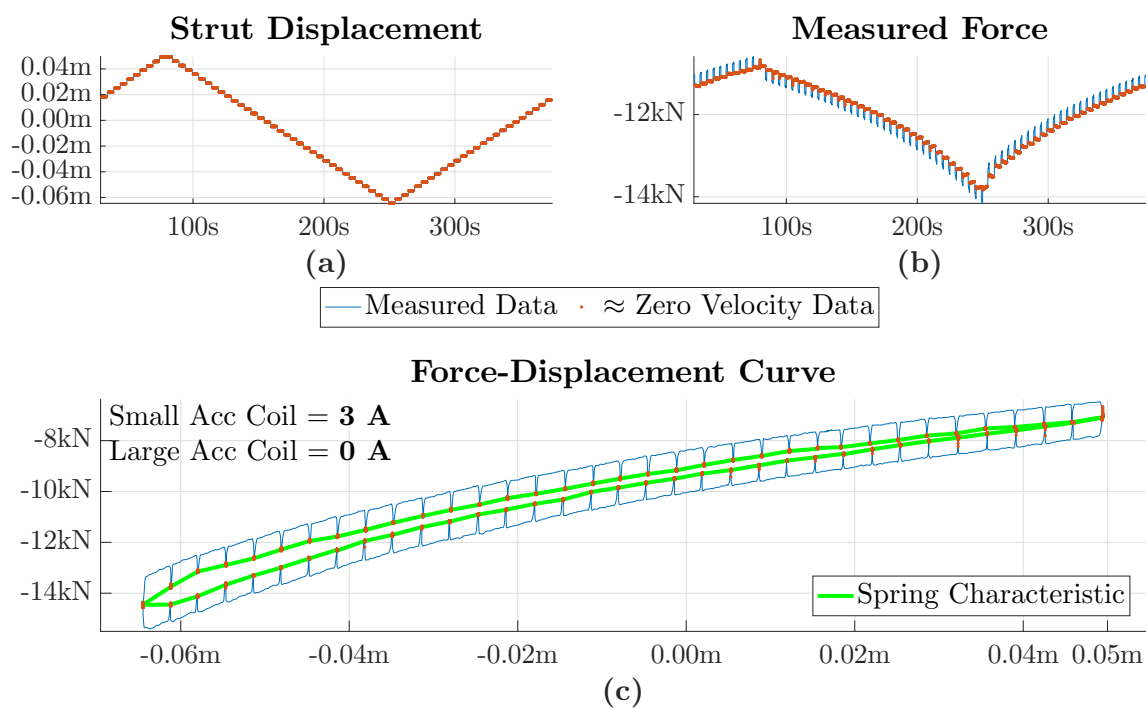


Figure 5.7: MR 4S₄ first Hard Spring Setting.

5.3.3 Results for the second Hard Spring Setting

Figure 5.8 (c) shows the characteristic of the second hard spring setting of the MR 4S₄. Here the active coil is located on the large accumulator side. The characteristic shown here is quite different from the previous two instances in the sense that there seems to be much more hysteresis present.

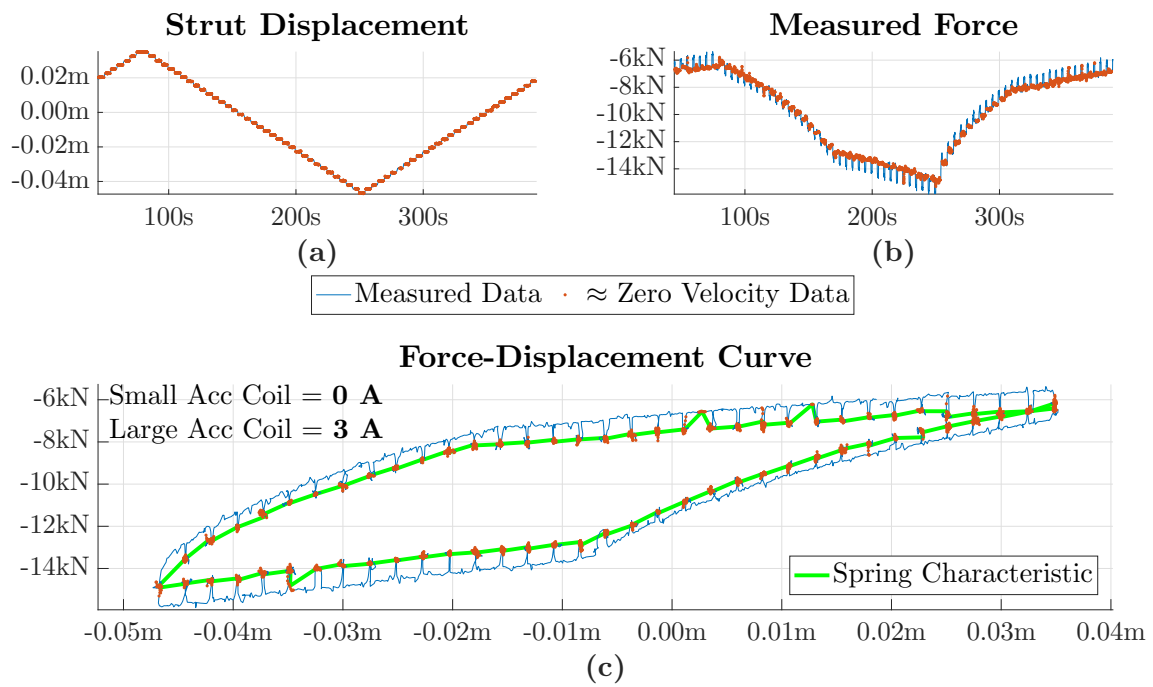


Figure 5.8: Measured pressure values for the second hard spring setting

In fact, hysteresis is not to blame, but rather a change in spring rate. Interestingly enough, a change in spring rate is clearly visible in [Figure 5.8 \(b\)](#) as a change in the slope of the measured force. This change in spring rate is explained using [Figure 5.9](#) as reference in [Table 5.3](#)

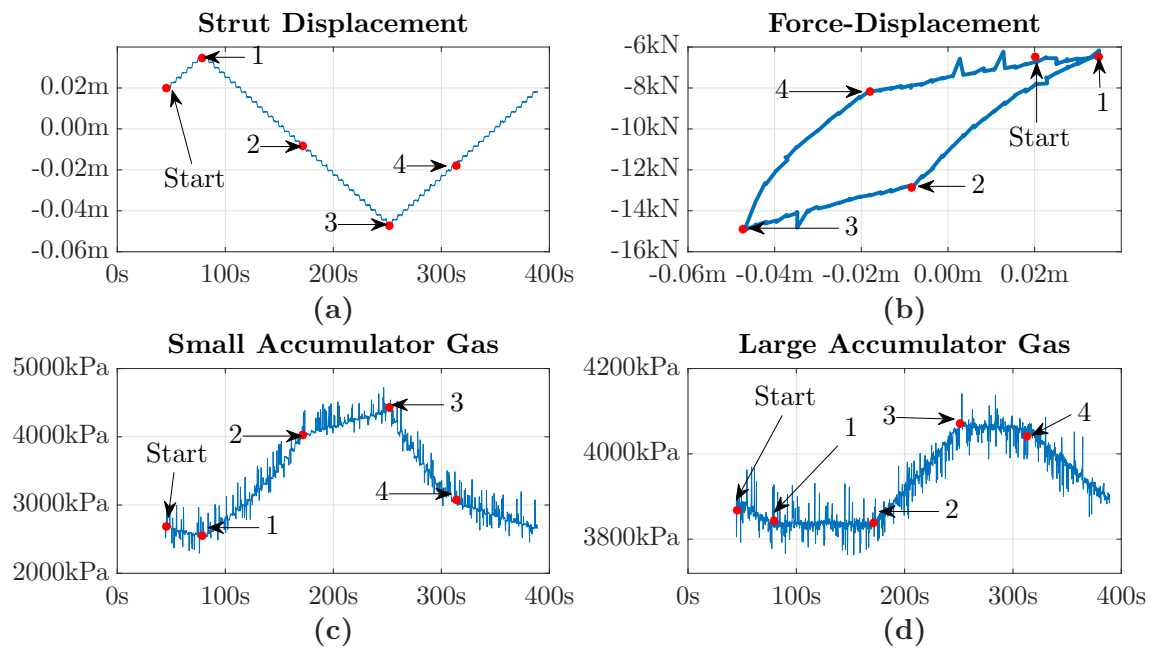


Figure 5.9: Measured pressure values for the second hard spring setting

5.3.4 Observations

The soft spring characteristic is the simplest of all three. It is just two gas springs in parallel being compressed and expanded. The test for the first hard spring characteristic were also quite successful. The MR valve of the small accumulator blocked the flow of fluid through it and the result is a slightly harder spring characteristic. The test for the second hard spring characteristic was not as successful as the MR valve could not block the flow of fluid for the whole stroke.

The first hard spring setting worked because the gas volume being compressed is much larger (i.e. large accumulator) than that of the small accumulator. Put simply, during the compression stroke of the main strut the pressure in the small accumulator will increase much faster.

However, the purpose of the study was to determine whether it was even remotely possible to change the spring rate of the system via the use of magneto-rheological (MR) valve. To show that this has been achieved, even though only for a fraction of the total stroke, the three discussed spring settings for the MR 4S₄ have been compiled together in [Figure 5.10](#).

Table 5.3: Explanation of [Figure 5.9](#)

Location	Description
1	This point is where the strut is extended to its maximum in this stroke. From Start to 1 , the slope of the spring characteristic, Figure 5.9 (b) , closely represents that of the Soft Spring.
1 - 2	Here the strut is compressed. From Figure 5.9 (d) it is seen that the gas pressure is constant. This results in a new slope for the spring characteristic, Figure 5.9 (b) .
2	Here a change in spring characteristic, Figure 5.9 (b) , is noted as well as a change in large accumulator gas pressure, Figure 5.9 (d) . This is due to the resistive force of the MR valve being championed by the pressure in the main strut.
2 - 3	Here the soft spring characteristic is seen again, Figure 5.9 (b) , as both gas volumes are gradually being compressed.
3	Turning point of the stroke, Figure 5.9 (a) .
3 - 4	Here the large accumulator gas pressure, (d) , is again constant and the harder spring characteristic is observed, Figure 5.9 (b) . Although the gas pressure is again steady, it is steady at a high pressure. This is because the resistive force of the MR valve is enough to block the flow.
4	Here the spring characteristics becomes soft again, Figure 5.9 (b) . The pressure in the main strut decreased enough to overcome the resistive force of the MR valve.

There is clearly a change in slope between the soft spring characteristic and the first hard spring characteristic. Even though the second hard spring characteristic is subject to a change in spring characteristic from very hard to soft, it is still clearly visible that the second hard spring characteristic has the highest slope of all.

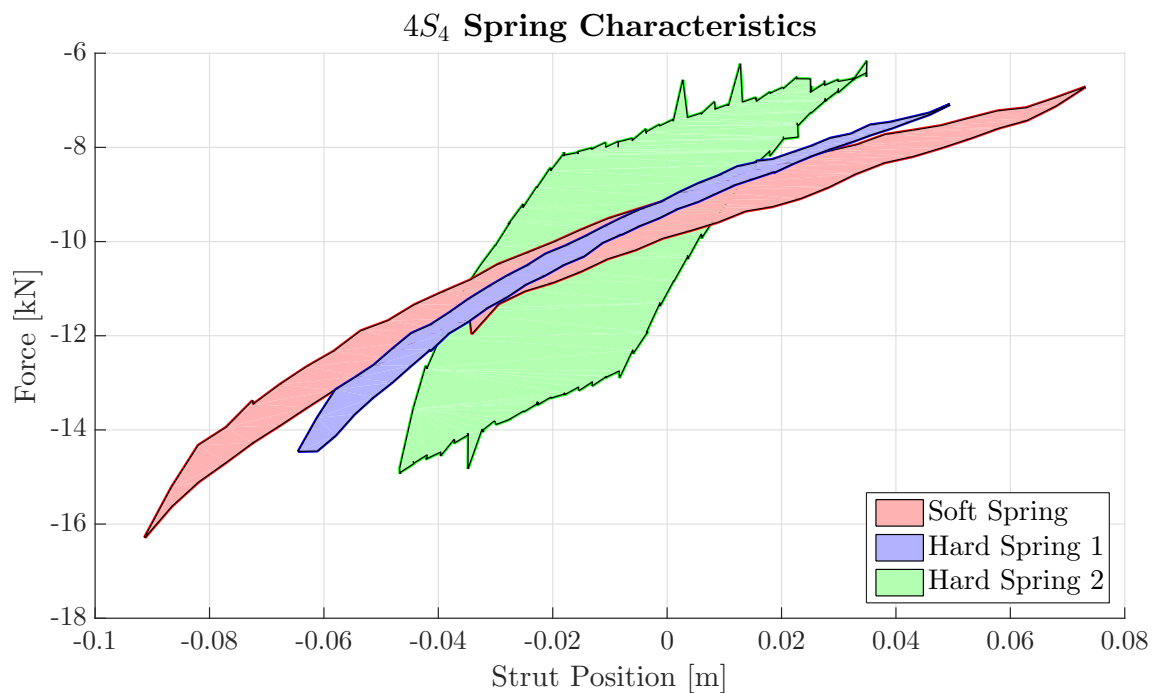


Figure 5.10: Three different spring settings.

5.4 MR $4S_4$ FLOW BLOCKING ABILITY

The ability of the system to block the flow of fluid is merely a measure to determine whether the system can lock up. The ability of the system lock up during a severe handling manoeuvre like the double lane change or moose test is a favourable feature to prevent excessive body roll.

Figure 5.11 shows the recorded data used to determine the resistive force of the system. To determine the flow blocking ability of the valve, the strut is positioned mid-stroke, Figure 5.11 (a), and the actuator controller is set to force control to achieve a constant force as measured on the actuator Figure 5.11 (b). Only the region with a constant velocity, Figure 5.11 (a) or constant strut position can be considered as the resistive force of the system. Note that the force given as input to the controller should be high enough to initially force fluid through the valves to ensure that full resistive ability of the system is measured.

Finally, assuming fluid is forced through both valves, the soft spring characteristic in Figure 5.6 is used to remove spring force from the measured force, Figure 5.11 (b), to reveal the resistive capability of the system.

Results from Flow Blocking Tests

Small Accumulator Coil = 3A

Large Accumulator Coil = 3A

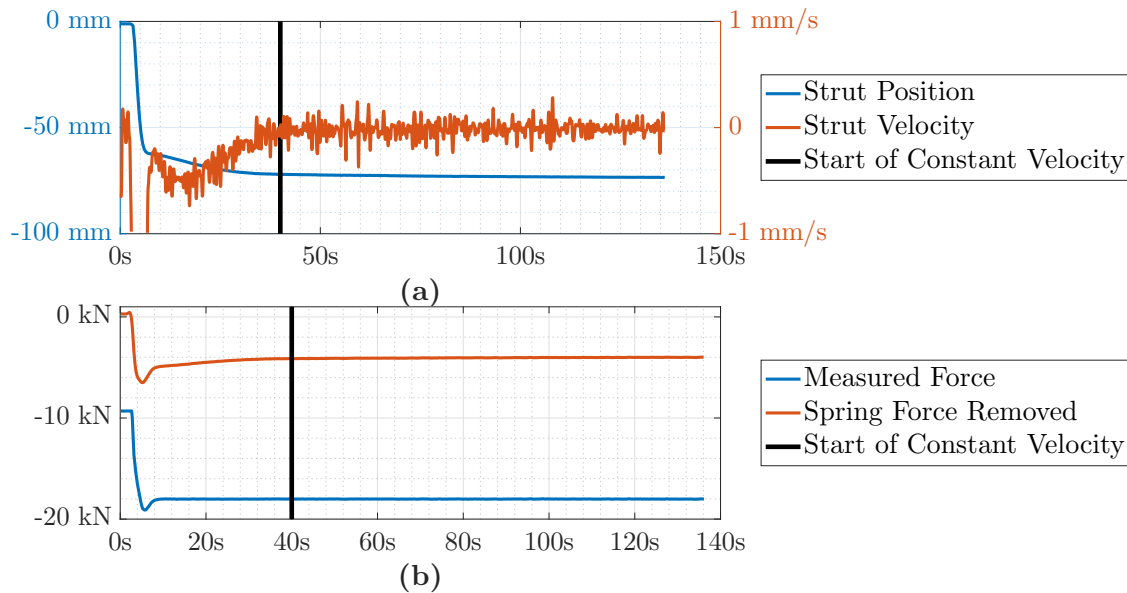


Figure 5.11: Typical recordings from the flow blocking tests.

This measurement method was implemented for a few different current settings to determine the resistive ability of each. Figure 5.12 shows the resistive ability for five different current settings respectively. Note that as the magnets approach saturation, the resistive ability of the system starts to converge to a maximum value. The resistive force is plotted against strut velocity as the flow through the valves cannot be truly zero. Even though the velocities are very close to zero, they are still subject to noise introduced during the differentiation of the position measurement. Interestingly enough the resistive ability of the system is also **4 kN**, the same as the valve in Chapter 3 and the valve by Meeser (2014), but at considerably lower velocities.

5.5 DAMPING TESTS

Actuator Input Signal Figure 5.13 shows the displacement curve that was used as input to the actuator. The triangular signal was chosen as it provides a large constant velocity region that aids in determining the damping characteristics of the system.

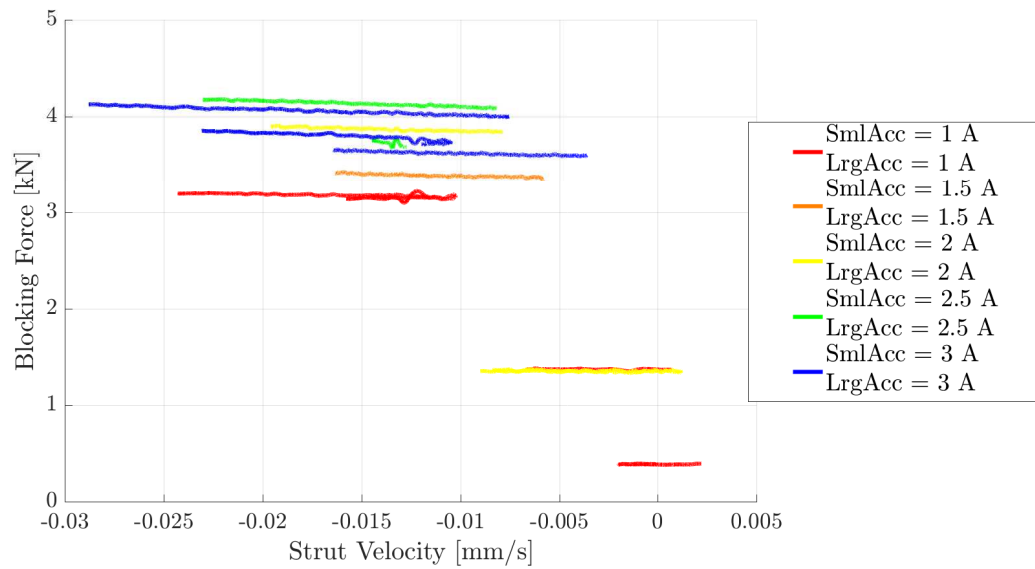


Figure 5.12: Ability of the combined valves to resist the flow of fluid.

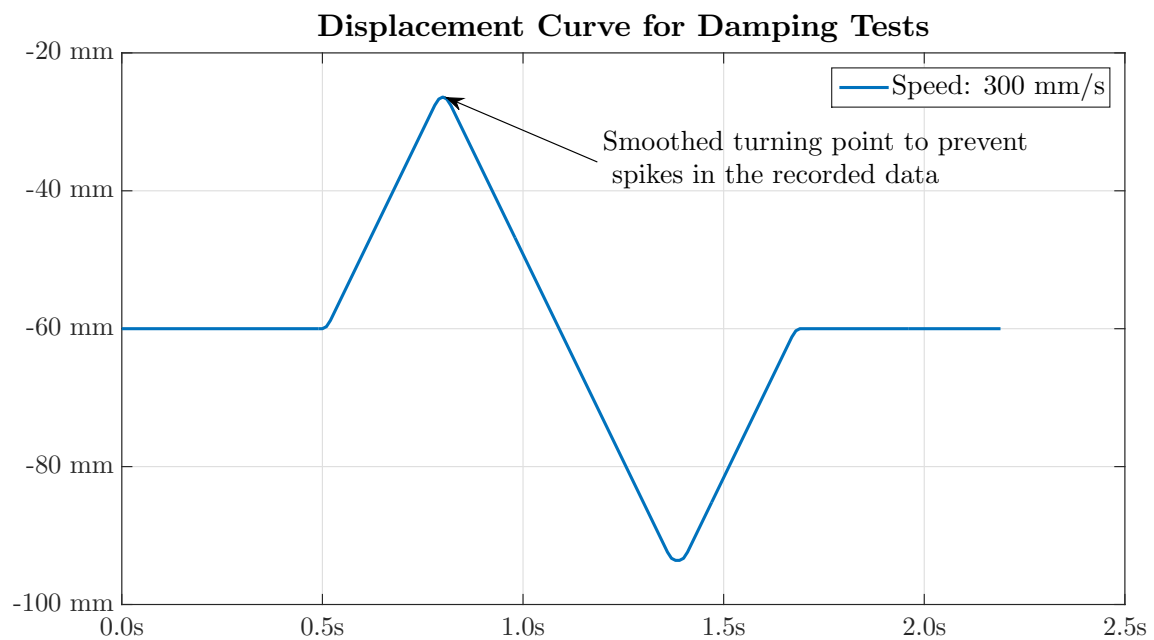


Figure 5.13: Displacement Signal that was used as input to the actuator controller.

5.5.1 Floating Piston Friction

One of the unknowns in the original version of the $4S_4$ by Els (2006) was the floating piston friction and the effect that friction has on the characteristics of the system. From observation in the section on spring characteristics, the floating piston friction is once again a cause

for concern. [Figure 5.14](#) presents the characteristic curves of the piston friction for each accumulator. These friction characteristics were determined from the difference in pressure data before (MR Fluid Pressure) and after (Gas Pressure) the piston. From these curves it is clear that the friction of the floating piston in the small accumulator is higher than that of the large accumulator. This confirms the conclusion made from the spring characteristics.

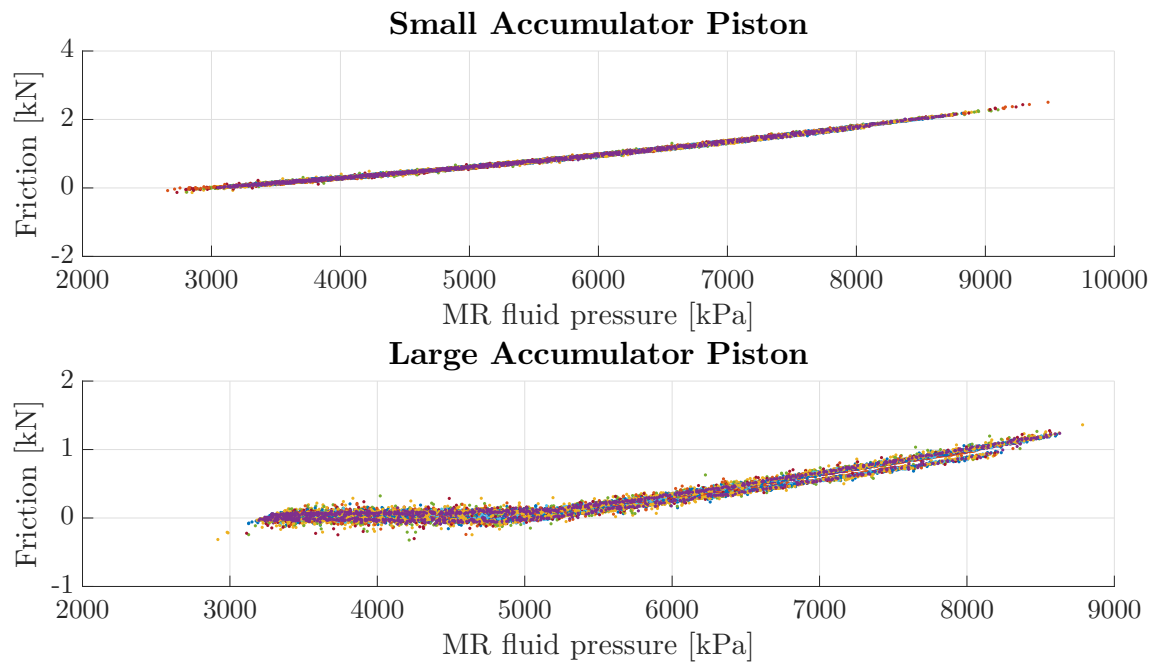


Figure 5.14: Accumulator Floating Piston Friction determined from Off-State damping data.

5.5.2 Estimated Spring Characteristic

The Force-Displacement curve is one way to visualize the damping characteristic of a suspension. Using the off-state damping characteristics, the original force-displacement data was corrected by removing the effects of the floating piston friction to yield a surprisingly close correlation with the measured soft spring characteristic determined above (assuming that the spring characteristic is the mean line through the force-displacement data). To correct for the floating piston friction a simple analogy of two resistive elements in parallel was used, where the total resistive force was obtained by

$$R_T = \frac{R_1 R_2}{R_1 + R_2} \quad (5.1)$$

[Figure 5.15](#) shows the original data, the corrected data, as well as the measure spring char-

acteristic. Keeping in mind that the tests for the spring characteristics and the damping tests were not consecutively performed, it is possible that some gas in the system may have escaped which may explain the slight difference in the characteristics.

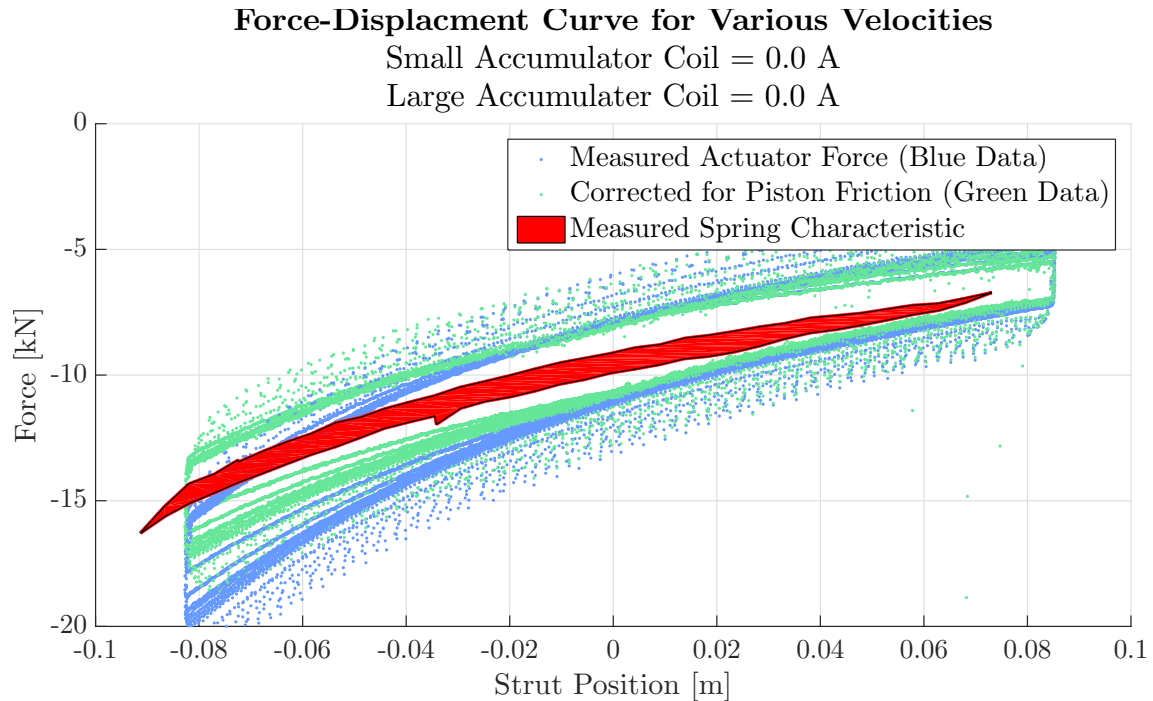


Figure 5.15: Force-Displacement data showing it is possible to determine the spring characteristics from damping data.

5.5.3 MR $4S_4$ Damping Characteristics

Figure 5.16 shows the results from the damping tests performed on the MR $4S_4$ prototype. Velocities ranging from below 10 mm/s to above 400 mm/s were tested. These velocities produce flow rates from 0 to 1 litres per second approximately. The following coil currents were tested in various combinations:

Small Accumulator Coil	1.0	1.5	2.0	2.5	3.0	3.5
Large Accumulator Coil	1.0	1.5	2.0	2.5	3.0	3.5

As is seen from the table above, currents between 0 A and 1 A were not tested as the power supply did not allow for current setting much lower than 1 A for each channel.

An interesting trend in the force-velocity response that can be seen from Figure 5.16 is that

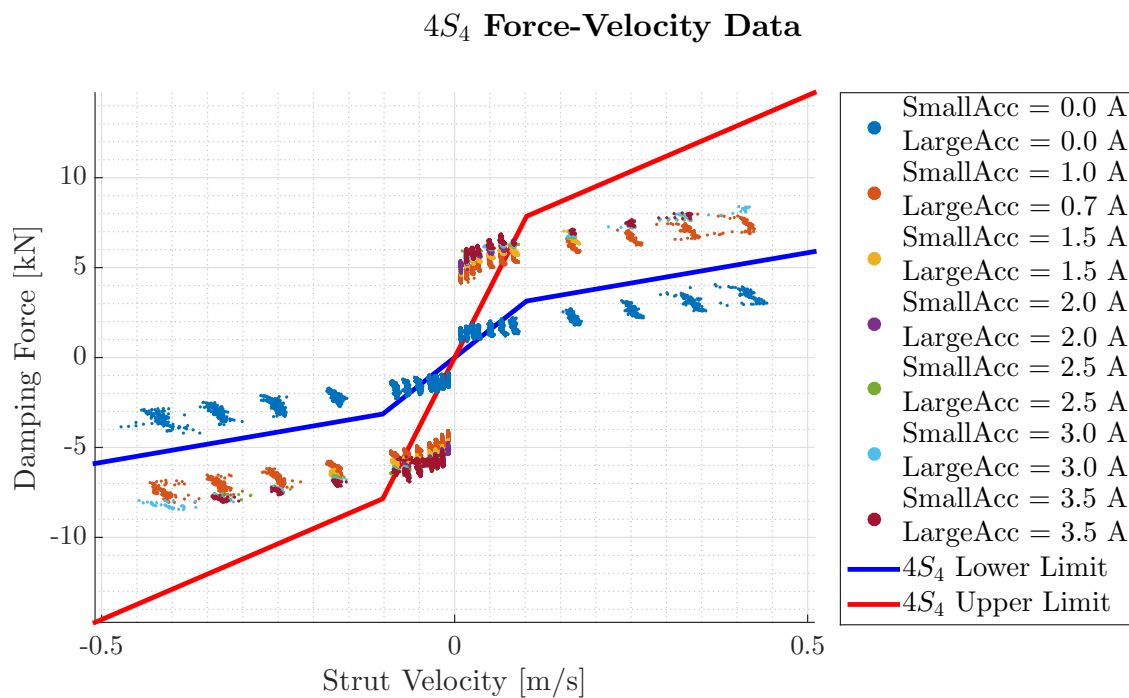


Figure 5.16: Force-Velocity Relationship of the MR 4S₄ Prototype for various current settings.

at low velocity, the damping force is much higher than expected and doesn't really decrease to zero as much as desired. This was also the case in chapter 3.

To determine the damping force for each test the measured actuator force had to be used. Even though the pressure data is available to determine the pressure drop over each valve, the flow rate through each valve is still unknown. Figure 5.17 shows how the damping force for each test was obtained. Using the force-position data a mean curve was fitted (estimated spring characteristic). The estimated spring characteristic is then removed from the force-position data to yield the damping force.

This method is however only valid when both magnets have the same current. The assumption is that both valves are identical and that the difference in flow rate between the two valves are small enough. It is quite difficult to determine the damping force when the two magnet currents are unequal. Figure 5.18 shows why it is difficult to determine the damping force, this is because for a single velocity you would have two different damping forces and a change in spring characteristic.

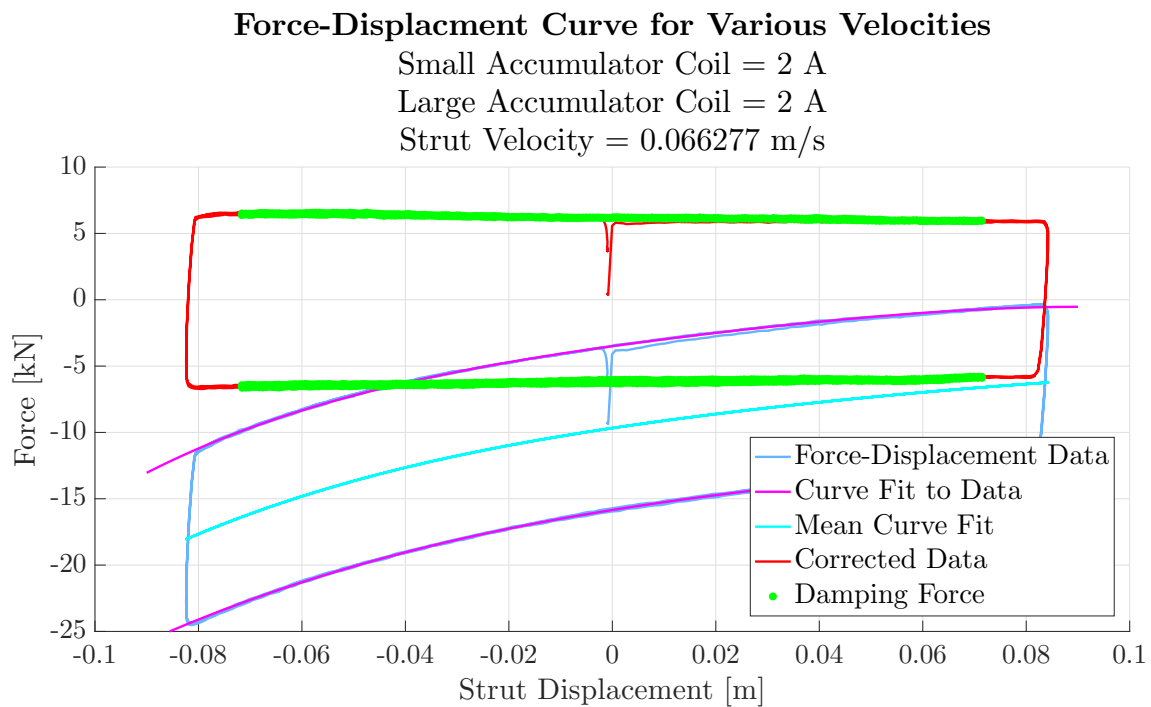


Figure 5.17: Force-Displacement Relationship of the MR 4S₄ Prototype showing how the damping data was extracted.

Why this happens can be better explained with [Figure 5.19](#) that shows the pressure of the MR Fluid between the valve and floating piston for the Small [Figure 5.19 \(a\)](#) & Large [Figure 5.19 \(b\)](#) accumulators respectively. Looking at [Figure 5.19 \(b\)](#) it can be seen that for a short period there is no change in pressure or rather no fluid flow through the valve. In this short period both the spring rate and damping force of the system is influenced.

5.6 CUSTOM PRESSURE SENSORS

[Figure 5.20](#) shows the results from the strain gauge measurements on the accumulators (see [subsection 4.2.2](#)) for various applied coil currents to the large and small accumulator magnets. [Figure 5.20 \(a\)](#) & [\(b\)](#) represents the pressure-strain relationship for MR Fluid and Gas chamber on the small accumulator (Location 6 & 5 on [Figure 4.3](#)). [Figure 5.20 \(c\)](#) & [\(d\)](#) represents the pressure-strain relationship for MR Fluid and Gas chamber on the large accumulator (Location 3 & 2 on [Figure 4.3](#)).

It is evident that there is a correlation between the current applied to the small accumulator and the jump in the Pressure-Strain curve. However, as to the cause of the problem no further

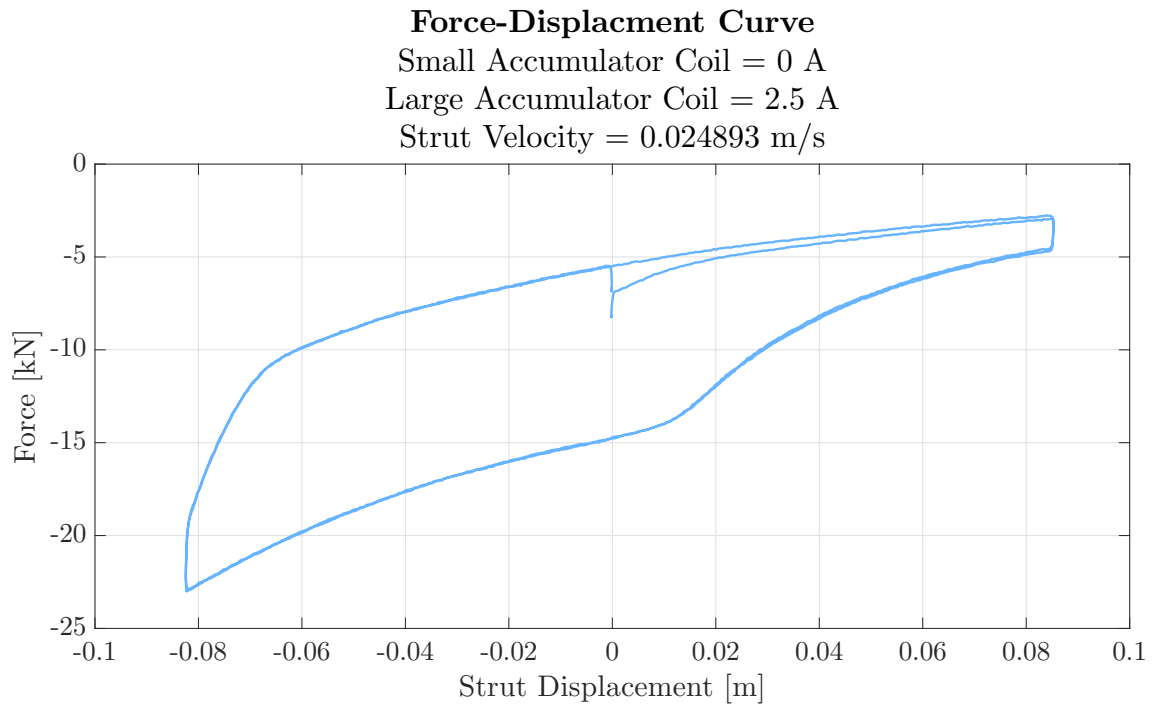


Figure 5.18: Force-Velocity Relationship showing a change in damping force mid-stroke.

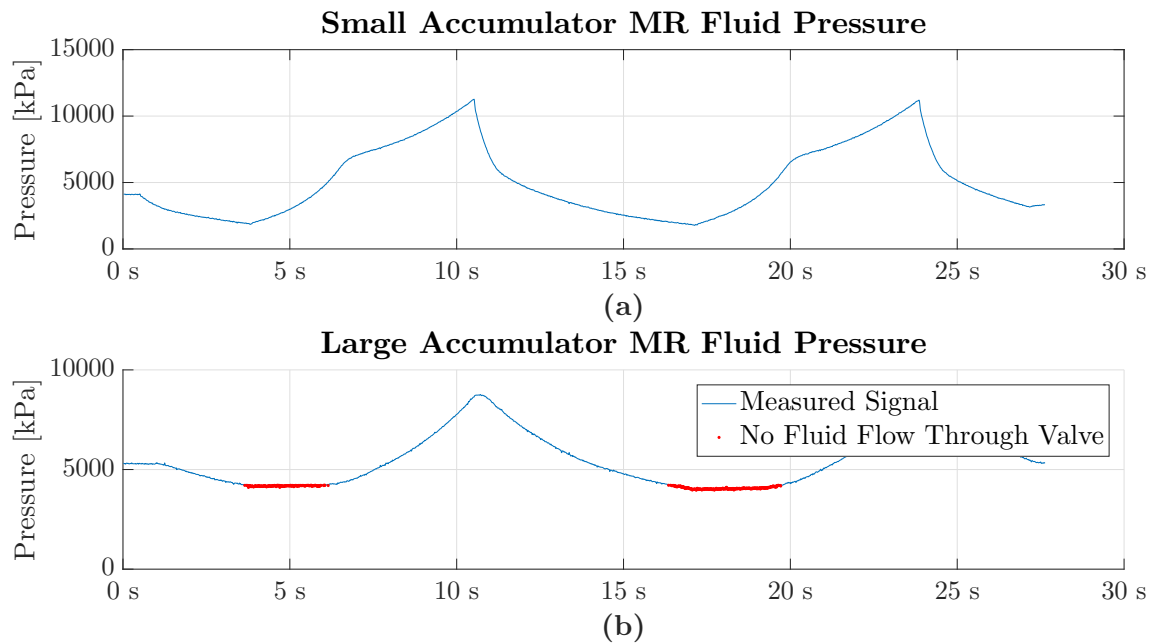


Figure 5.19: Small & Large Accumulator MR fluid Pressure showing how fluid flow is temporarily block through the valve of the small accumulator.

investigation was performed as this exercise was merely a proof of concept. Therefore, strain sensors can be used on the accumulators to gather more suspension data for better control

of the system.

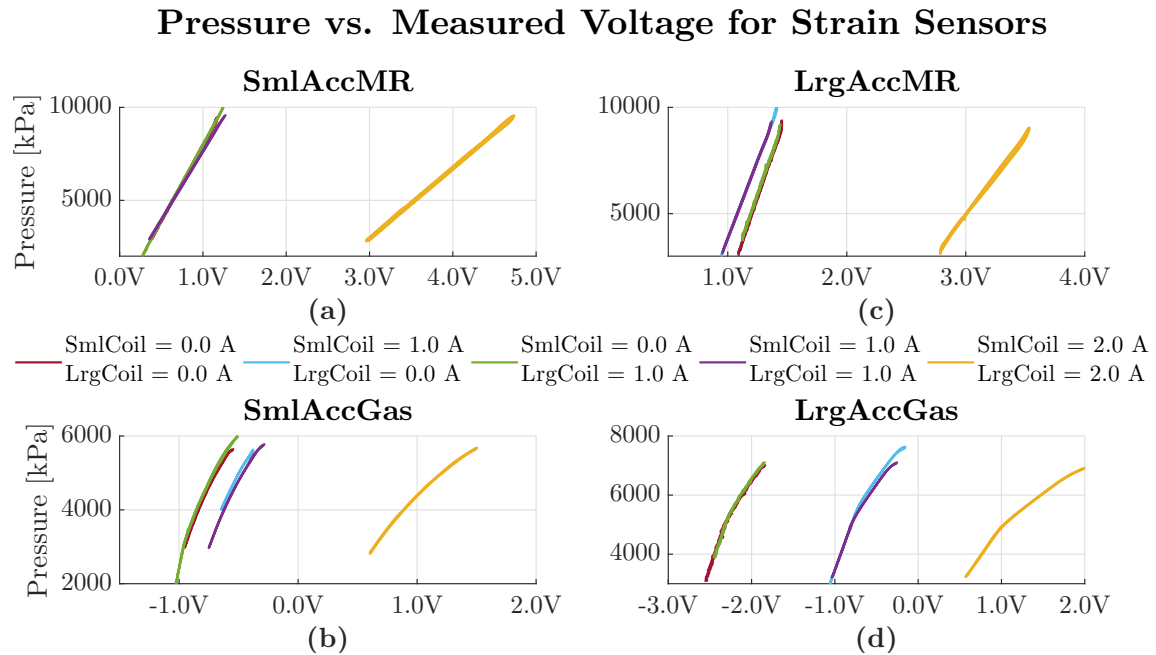


Figure 5.20: Pressure - Strain relation for all strain sensors.

5.7 CONCLUSION OF RESULTS

This concludes the section on the experimental results. It is seen that there was still a considerable amount of air as well as other various "play" in the system that required a few millimetres of compression before the bulk modulus of the system could be measured.

After determining that the dual channel power supply could be used for the response time tests, the results presented were quite unexpected. The isolated response time of the MR valve magnetic circuit at static conditions are worse than that of the solenoid valves used by [Els \(2006\)](#). The system response time is even worse, therefore an improvement in the design of the magnetic circuit is required as well as the design of the valve geometry to improve the system response time.

The spring characteristics and flow blocking ability of the $4S_4$ are linked in the sense that the higher resistive force each valve provide, the easier a higher spring rate can be maintained. Therefore, by decreasing the flow area of each valve a higher resistive force can be achieved.

The piston friction that was determined from the off-state damping data shows that the effect of friction can be quite significant. This effect is even further proven by the spring estimate that was extracted from the off-state damping data. Reducing friction should be a design requirement on the top of the list.

The damping forces of the current system are too low unfortunately whereas the first MR valve prototype had too high damping forces. It would seem that the combined damping capabilities of the two valves in the system produces a lower damping effect than expected mainly because the flow is split between the two valves and appropriate design changes needs to implemented. As for the higher than expected damping forces at low velocities, more work is still needed to better model the behavior of the MR fluid for a single valve in order to aid with the design of an entire suspension system.

CHAPTER 6

CONCLUSION AND RECOMMENDATIONS

The purpose of this study was to design and test a MR valve to replace the current solenoid valves in the $4S_4$ suspension system. This MR valve still had to be able to provide the necessary damping characteristics and also had to be able to block the flow of fluid during severe handling manoeuvres as well as successfully change spring characteristics. Another requirement is that the MR valve should have a comparable response time to that of the solenoid valves.

Unfortunately only some of the conditions were achieved, namely the two spring characteristics. The response time was much more worse than expected and the damping capability of the system is lower than what was hoped for.

6.1 RESPONSE TIME

It was quite fortunate that there was almost no difference between the response time measurements of the power supply and the battery and that the 63.2% response time of the MR fluid is in the region of $4ms$ as suggested by literature.

The response time of the system is currently too large for the suspension system to be implemented in vehicle tests. One method to reduce the response time is to decrease the gap width of the valve flow area. This is favourable in the sense that most of the improvements currently required for this system is linked to the gap width of the valve flow area. Reducing the gap width decreases the distance the magnetic flux needs to travel through a bad magnetic conductor.

The second method of improving the response time is to use a magnetic material with a higher magnetic permeability. These materials typically have large amount of nickel present in the alloy. The third improvement is a change in valve construction.

6.2 MAGNETIC CIRCUIT

The magnetic circuits of both prototypes are the same, but with different materials. If the same should be used again there is a small improvement to be made.

Figure 6.1 shows the current magnetic circuit layout and more specifically notice the Aluminium core. The purpose of the core is to act as an insulating element so that the magnetic flux is directed mostly through the **MR gap**. It may be possible to replace the Al core with a much thinner metal core. Figure 6.2 shows how this new magnetic circuit could possibly look by combining the two side cores and and the new thinner metal core into one element.

The reasoning behind this is simple. Magnetic flux is generated within the central core and the magnetic elements around the coil provide a return path for the magnetic flux. By bringing the coil closer to the central core more magnetic flux is generated in the central core due to the decreased magnetic resistance. This improvement is conditional to the correct design of the thinner metal core.

Ideally the coil should be also be exposed to MR fluid as the MR fluid is still a 5 – 9 **X** better magnetic conductor than air. This will increase the efficiency of the coil and the MR effect in the gaps.

6.3 DAMPING

In order for the system to be versatile enough for both ride comfort and handling requires a specific damping range. Unfortunately the desired range of damping was not achieved for the current iteration of the suspension system, but the solution is known. A change in valve geometry would definitely shift the current damping range up towards the desired range.

A cause for concern with MR based dampers is the high damping forces at low velocities which influences the secondary ride of the vehicle, which will only be worse once the necessary design

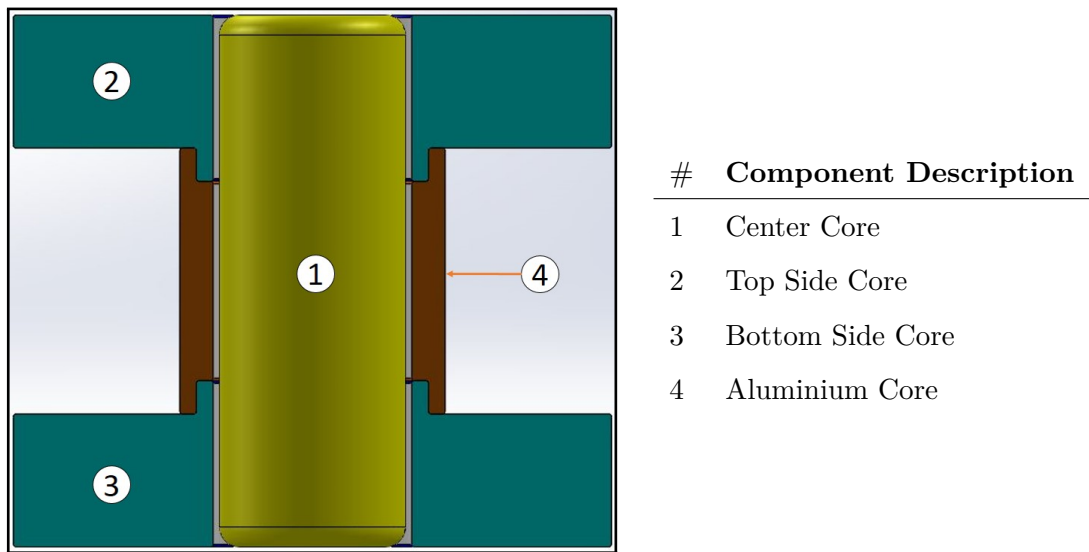


Figure 6.1: Current Construction of the Magnet.

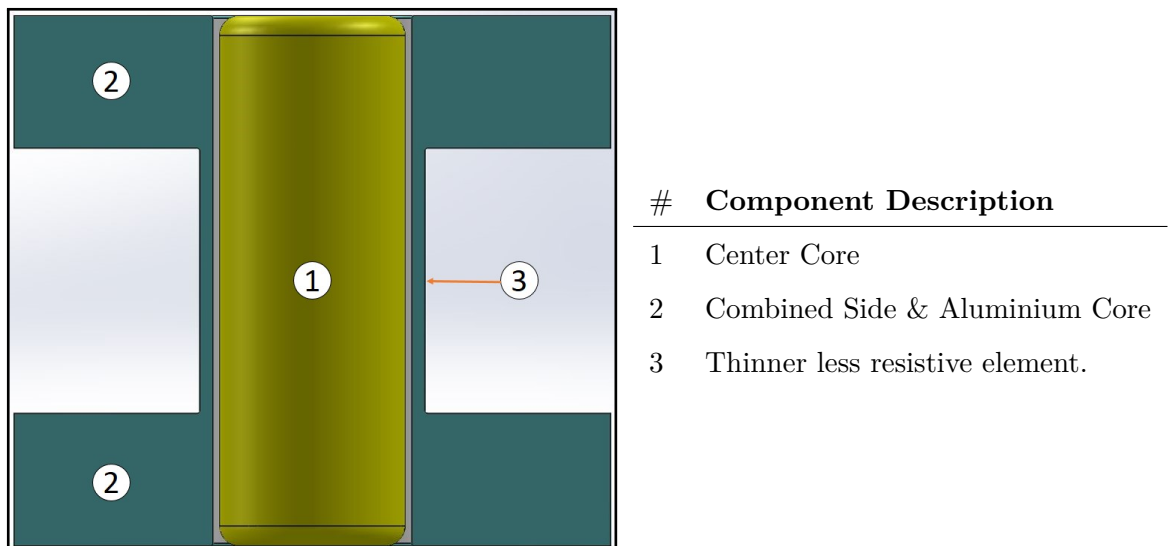


Figure 6.2: Proposed new construction of the Magnet.

changes are implemented to correct the damping range. A solution is required which will give lower damping forces at these velocities while still keeping the same damping range.

Figure 6.3 presents a possible solution in the form of a bypass valve which could be activated when these low damping forces are required. Using the already existing inner core (yellow) a hole is drilled through the center of the core (one is already present, it was used to measure pressure in the chamber below the valve) and hole in the side, fluid can be allowed past the

annular flow area to decrease the damping force.

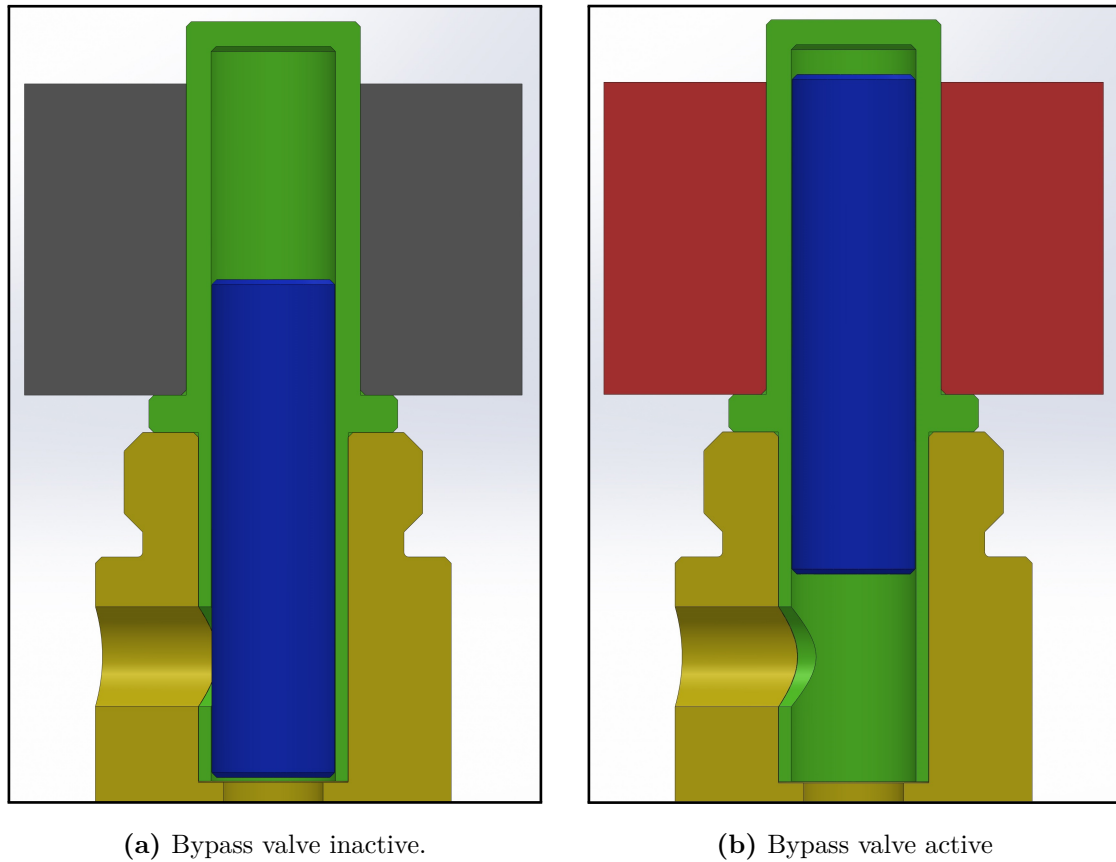


Figure 6.3: Design of a possible solution for the high recorded damping forces at low speeds by means of a bypass valve.

Overall the MR valve technology still seems to provide a good range of damping. An interesting observation is the large gap in [Figure 5.16](#) between the 0 A setting and 1 A setting. This indicates a sudden increase in magnetic field strength which would make control in that region slightly more difficult. The second observation is that the magnetic circuit is starting to saturate at around 2 Amps. This can be seen by only slight increase in damping force for higher currents.

6.4 STRAIN SENSORS

[Figure 5.20](#) shows that it is indeed possible to use the strain gauges as pressure sensors as there is a clear relationship between the pressure and the measured strain even though there is a correlation between the offset of the measured strain and the applied magnetic field. The

only improvement needed is that the strain sensors should be better protected with shielded cables, or amplifying the low level voltages much closer to the strain gauges.

With a complete rebuild on the $4S_4$ system the sensor locations can be changed to allow for better and more measurements, than the current one implemented on the Land Rover Defender 110. For example, sensor locations 1, 2 and 5 on [Figure 4.3](#) would be ideal locations (Main strut and the two gas volumes) especially if the floating pistons in the accumulators can be replaced with flexible membranes to separate the gas and MR fluid. This would also eliminate the need for a load cell on the main strut, as the suspension force can then be determined from the main strut strain sensor.

[Figure 6.4](#) shows an example implementation for the strain gauges. Ideally a small pocket is machined into the area where the pressure needs to be measured. The strain voltage is amplified and filtered directly in the pocket so that only a high level output is present. Further more the strain gauges and the electronics is protected from the elements and EMF noise with a cap that is grounded to the supply through a large resistance.

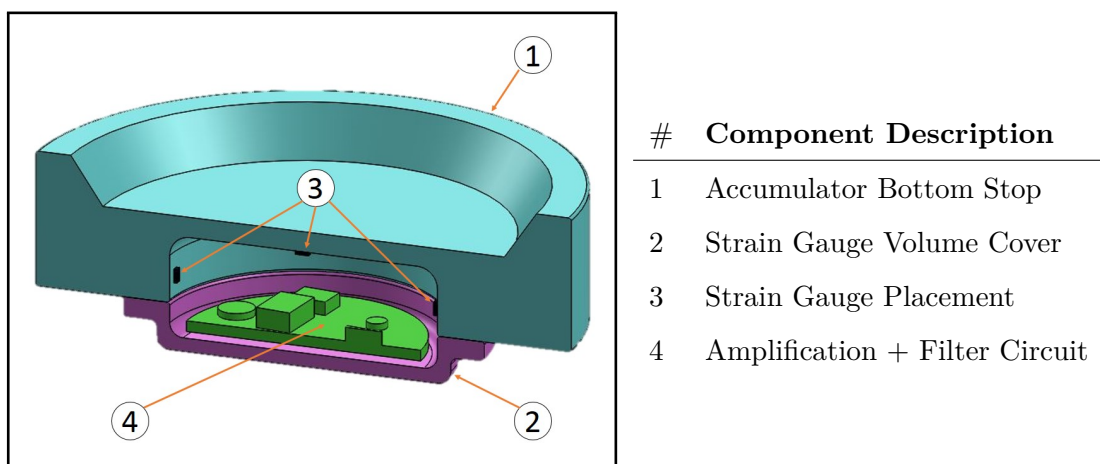


Figure 6.4: Possible implementation of strain gauge sensors to avoid interference.

REFERENCES

Carlson, J., Catanzarite, D., St. Clair, K., 1996. Commercial magneto-rheological fluid devices. *International Journal of Modern Physics B* 10 (23n24), 2857–2865.

Carlson, J. D., 2005. Mr fluids and devices in the real world. *International Journal of Modern Physics B* 19 (07n09), 1463–1470.

Carlson, J. D., Chrzan, M. J., Jan. 11 1994. Magnetorheological fluid dampers. US Patent 5,277,281.

Delphi, C., 2005. Delphi magneride.

URL <http://delphi.com/shared/pdf/ppd/chsteer/magneride.pdf>

Dixon, J., 2007. *The shock absorber handbook*. John Wiley & Sons.

Duclos, T. G., 1988. Design of devices using electrorheological fluids. Tech. rep., SAE Technical Paper.

Els, P. S., 2006. The ride comfort vs. handling compromise for off-road vehicles. Phd, University of Pretoria.

URL <http://www.up.ac.za>

Jolly, M. R., Bender, J. W., Carlson, J. D., 1999. Properties and applications of commercial magnetorheological fluids. *Journal of Intelligent Material Systems and Structures* 10 (1), 5–13.

Liquids Research, L., Nov. 2014. Magnetorheological fluids. [Online]. Available at.

URL http://liquidsresearch.co.uk/en-GB/magnetorheological_fluids-51.aspx

LORD, Nov. 2014. Mr faq's. [Online]. Available at.

URL <http://www.lordmrstore.com/faq>

MagWeb, Nov. 2014. Free bh curves. [Online]. Available at.

URL <http://magweb.us/free-bh-curves/>

Meeser, R. F., 2014. Magneto-Rheological (MR) Damper Design for Off-Road Vehicle Suspensions with Flow Blocking Ability. Master's thesis, University of Pretoria.

MSC, Nov. 2014. Marc student edition. [Online]. Available at.

URL <http://web.mscsoftware.com/Academia/Student-Center/Marc-And-Mentat.aspx>

Phillips, R. W., 1969. Engineering applications of fluids with a variable yield stress. Ph.D. thesis, University of California, Berkeley.

Seung-Bok, C., Young-Min, H., 2012. Magnetoreheological Fluid Technology. CRC Press.

Thoesson, M. J., Uys, P., Els, P. S., Snyman, J. A., 2009. Efficient optimisation of a vehicle suspension system, using a gradient-based approximation method, part 2: Optimisation results. *Mathematical and Computer Modelling* 50 (9), 1437–1447.

Ulaby, F. T., Michielssen, E., Ravaioli, U., 2010. *Fundamentals of applied electromagnetics*. Prentice Hall.

Wereley, N. M. (Ed.), 2014. *Magnetorheology*. RSC Smart Materials. The Royal Society of Chemistry.

URL <http://dx.doi.org/10.1039/9781849737548>